UNCLASSIFIED
SECURITY CLASSIFICATION OF THIS PAGE

REPORT DOCUMENTATION PAGE

Form Approved
OMB No 0704 0188

1a REPORT SECURITY CLASSIFICATION UNCLASSIFIED	1b RESTRICTIVE MARKINGS
	3 DISTRIBUTION/AVAILABILITY OF REPORT This document has been approved for public release and sale; its distribution is unlimited.
AD-A212 688	5 MONITORING ORGANIZATION REPORT NUMBER(S) Technical Report #19
IBM Research Report RJ6992	
6a NAME OF PERFORMING ORGANIZATION IBM Research Division Almaden Research Center	6b OFFICE SYMBOL (If applicable)
6c ADDRESS (City, State, and ZIP Code) 650 Harry Road San Jose, CA 95120-6099	7a NAME OF MONITORING ORGANIZATION Office of Naval Research
8a NAME OF FUNDING/SPONSORING ORGANIZATION Office of Naval Research	8b OFFICE SYMBOL (If applicable)
8c ADDRESS (City, State, and ZIP Code) Chemistry Division, Code 1113 Arlington, VA 22217	7b ADDRESS (City, State, and ZIP Code) Chemistry Division Code 1113 Arlington, VA 22217
	9 PROCUREMENT INSTRUMENT IDENTIFICATION NUMBER N00014-84-C-0708, 4131022
	10 SOURCE OF FUNDING NUMBERS PROGRAM ELEMENT NO / PROJECT NO / TASK NO / WORK UNIT ACCESSION NO

11 TITLE (Include Security Classification)
Optical Detection and Probing of Single Dopant Molecules of Pentacene in a p-Terphenyl Host Crystal by Means of Absorption Spectroscopy

12 PERSONAL AUTHOR(S)
L. Kador, W.E. Moerner & D.E. Horne

13a TYPE OF REPORT	13b TIME COVERED	14 DATE OF REPORT (Year, Month, Day)	15 PAGE COUNT
Interim Technical	FROM _____ TO _____	1989, August 31	52

16 SUPPLEMENTARY NOTATION
Submitted for publication in the Journal of Physical Chemistry

17 COSATI CODES			18 SUBJECT TERMS (Continue on reverse if necessary and identify by block number)
FIELD	GROUP	SUB-GROUP	Single Molecule Detection FM Spectroscopy Pentacene in p-terphenyl Ultrasensitive Spectroscopy

19 ABSTRACT (Continue on reverse if necessary and identify by block number)

See Reverse

20 DISTRIBUTION/AVAILABILITY OF ABSTRACT ☒ UNCLASSIFIED/UNLIMITED ☐ SAME AS RPT ☐ DTIC USERS	21 ABSTRACT SECURITY CLASSIFICATION UNCLASSIFIED
22a NAME OF RESPONSIBLE INDIVIDUAL Dr. W.E. Moerner	22b TELEPHONE (Include Area Code) (408) 927-2426

DD Form 1473, JUN 86 Previous editions are obsolete SN 0102-LF-014-6603 UNCLASSIFIED

OFFICE OF NAVAL RESEARCH

Contract N00014-84-C-0708

R&T Code 4131022

Technical Report No. 19

Optical Detection and Probing of Single Dopant Molecules of Pentacene in a p-Terphenyl Crystal by Means of Absorption Spectroscopy

by

L. Kador, D. E. Horne, and W. E. Moerner

Prepared for Publication

in

Journal of Physical Chemistry

IBM Research Division
Almaden Research Center
650 Harry Road
San Jose, California 95120-6099

August 31, 1989

RJ 6992 (66529) 8/31/89
Physics

OPTICAL DETECTION AND PROBING OF SINGLE DOPANT MOLECULES OF PENTACENE IN A *p*-TERPHENYL HOST CRYSTAL BY MEANS OF ABSORPTION SPECTROSCOPY

L. Kador*, D. E. Horne, and W. E. Moerner

IBM Research Division

Almaden Research Center

San Jose, California 95120

ABSTRACT: Using a combination of laser frequency-modulation absorption spectroscopy and either Stark, longitudinal ultrasonic, or transverse ultrasonic internal modulation, the optical absorption spectrum of a single impurity molecule of pentacene in *p*-terphenyl crystal may be measured at liquid helium temperatures. The general properties of this detection method are illustrated by first applying the technique to the detection of persistent spectral holes in the pentacene/*p*-terphenyl system. Selection of a single absorber for measurement is accomplished by tuning the probing laser far out into the wings of the inhomogeneously broadened 0-0 absorption lines for either the O_1 or O_2 sites. The single-molecule line shape is similar to that predicted by a simple model of the double-modulation process. The approximate amplitude of the single-molecule signals suggests that triplet bottleneck power broadening is suppressed far out in the wings of the inhomogenous line. This work probes the ultimate $N = 1$ limit of the statistical fine structure present in all inhomogenous absorption lines.

*Present address: University of Bayreuth, Bayreuth, West Germany

I. Introduction

Optical absorption lines of impurity molecules or ions in a solid matrix are usually subject to inhomogeneous broadening [1, 2] thereby reflecting various imperfections in the structure of the host material. The inhomogeneous distribution can be roughly described by a Gaussian profile, since the exact position of each individual absorption line depends on many random parameters, namely the position and orientation of the absorber with respect to those of all the surrounding molecules in the matrix. However, as has been demonstrated recently [3-5] a closer examination shows that a fundamental statistical fine structure (SFS) is superimposed on the smooth Gaussian curve. This fine structure is due to statistical fluctuations of the number of individual absorption lines from one frequency interval within the inhomogeneous distribution to the next. According to fundamental laws of statistics, the fluctuations in the number of absorption lines per homogeneous linewidth, N_H , are equal to the square root of its average value,

$$\Delta N_H = \sqrt{\overline{N}_H} \ , \tag{1}$$

in the limit $\overline{N}_H >> 1$. Since the absorption coefficient α is proportional to N_H , the SFS, which corresponds to the fluctuations in α, is largest in highly doped samples and at the center of an inhomogeneous line (as long as the concentration is not too large). The relative magnitude of the SFS, $\Delta N_H/\overline{N}_H$, on the other hand, increases with decreasing impurity concentration. Finally, at extremely low concentrations or far out in the wings of an inhomogeneous line, the absorption spectrum consists only of individual molecular absorption lines, so that

$$\Delta N_H = N_H \ . \tag{2}$$

This is the limit $\overline{N}_H << 1$. In the present paper we show that absorption signals due to single molecules in a solid matrix can be detected, corresponding to the attainment of the ultimate $N_H = 1$ limit of SFS. Our model system is pentacene in *p*-terphenyl single crystals.

In the past few years, several ultrasensitive experiments for the optical detection and spectroscopy of single absorbers in various environments were performed[5-15]. Most of the work was concentrated on single atomic ions confined in electromagnetic traps in vacuum. For example, by detecting the fluorescence from trapped ions slowed by laser-cooling, a variety of interesting quantum jump[6] and photon antibunching[7-9] phenomena were observed that test our understanding of basic atomic and quantum physics. For the case of Hg^+, it was even possible to determine the radiative transition rates between the four lowest energy levels from the quantum jumps of a single ion[10]. In the same system, Doppler sidebands of one specific transition in a single ion due to secular motion in the pseudopotential of the rf trap were detected[11]. While most of these experiments involved the measurement of the fluorescence from the confined ion, a successful absorption experiment was also reported[12].

In condensed matter, the experimental techniques for detecting single absorbing centers have not been developed as far as for the case of trapped ions in vacuum. Important early results included the detection of single viruses and bacteria[13] and single protein molecules with multiple chromophores[14] in liquid media by using novel optical traps and hydrodynamic focusing techniques, respectively. In the solid state, the detection of the fluorescence signal from as few as five Sm^{2+} ions in a CaF_2 crystal at 77K at a single fixed frequency has been reported[15]. One advantage of performing ultrasensitive optical experiments in a solid is the fact that the absorbing centers are effectively trapped by the host matrix and, therefore, inherently show "static" behavior without any Doppler or recoil effects, although the centers do interact with host phonons. The optical spectroscopy of a single impurity ion or molecule in a low-temperature solid could, furthermore, provide a new tool for the study of local guest-host interactions without the conventional averaging over as many as 10^4 to 10^{16} more-or less-equivalent sites. However, detection of single absorbers in a solid presents problems not present in the case of single ions in vacuum. For fluorescence experiments, it is difficult to detect the signal from a single absorber in the Rayleigh and/or Raman background from the large number ($10^{10} - 10^{18}$) of host molecules or ions in the probing

volume. In order to circumvent the problem of Rayleigh or Raman scattering, we used two high-sensitivity zero-background forms of absorption spectroscopy, laser frequency Stark (FM Stark) and laser frequency ultrasonic (FM/US) double modulation, which are described in the next section. Furthermore, since the sample must be kept at low temperatures in a cryostat, the problem of mechanical vibrations and/or slow motion due to thermal expansion or contraction must be solved.

One crucial issue for single-molecule spectroscopy in solids is the method of selection of a single absorbing center. Successive dilution of the doped host material is one method of achieving low concentrations; however, we chose to use the inhomogeneous line broadening effect directly as shown in Figure 1. The left side of the figure shows an inhomogeneous line composed of many discrete homogeneous (usually Lorentzian) absorption profiles; the overall shape of the inhomogeneous line is Gaussian in many cases. At a laser wavelength near the center of the inhomogeneous line, many molecules are in resonance with the laser, and the absorption profile shows the characteristic SFS reported earlier[4]. However, far out in the wings of the line, fewer and fewer centers are in resonance with the laser. It is clear that for a wavelength sufficiently far from the line center, the number of molecules in resonance within the focal volume can be reduced to one, or even less than one. *This is the method* whereby we reduced the concentration of molecules in resonance to unity. The method has the advantage that by tuning the laser to the center of the line, strong SFS signals are available for optimization of the detection conditions. Then by tuning to the wings of the line, single molecule spectra can be obtained, and by tuning out even further, a background level that should be similar to an undoped sample may be recorded.

In the following, we present experimental data describing the optical detection and spectroscopy of individual pentacene molecules in a *p*-terphenyl single crystal at 1.5K. First results of this work were published recently[16]. Section II describes the experimental details,

Section III the theory of the lineshape and the expected single-molecule signal size, and Section IV presents the results and discussion of our measurements.

II. Experimental

A. Frequency Modulation Spectroscopy

The basic spectroscopic technique that we used for the detection of SFS and single-molecule signals is frequency-modulation (FM) spectroscopy (FMS), a low-background method that was first described several years ago[17]. The method operates by sensing the conversion of a frequency-modulated light beam into an amplitude-modulated beam by a narrow spectral feature. The basic operation of the technique is illustrated schematically in Figure 2. First, a single-frequency (tunable) laser beam is passed through an optical phase modulator (an electrooptic crystal such as $LiTaO_3$) which is fed by a radio frequency (rf) source. A key advantage of FMS is that the modulating frequency ω_m is in the MHz frequency range or higher so that the laser noise at ω_m consists in most cases of only quantum shot noise. In the limit of low rf power and, hence, low modulation index, only two sidebands around the laser carrier frequency ω_c located at $\omega_c \pm \omega_m$ are appreciable in amplitude. One of these sidebands oscillates in phase with the central (carrier) line, the other out of phase by 180°. When no sample is present to disturb the equality of the two sidebands, the beat signals at ω_m due to the carrier mixing with each of the sidebands at the detector cancel, giving no signal at ω_m. This is simply a frequency-domain statement of the fact that an ideal phase-modulated beam has no amplitude modulation. The situation changes, however, when the light passes through a sample containing narrow absorption features. As long as the spectral feature is not much wider than the sideband spacing, the two sidebands are attenuated by different amounts, and, as a result, a photocurrent appears at ω_m at the fast photodetector. Thus, another virtue of FM spectroscopy lies in its sensitivity only to narrow absorbing features and the rejection of broad signals. For example,

FMS is capable of detecting the narrow SFS structures on an inhomogeneous line, but is insensitive to the broad inhomogeneous background absorption [3,4]. The modulated photocurrent at ω_m is phase-sensitively detected using a rf mixer. Either the sample absorption or dispersion may be probed by proper choice of phase.

There is, however, a serious practical limitation to the sensitivity of a real FM experiment, namely residual amplitude modulation (RAM) in the modulator crystal or in other optical components which causes a frequency-dependent imbalance in the two sideband amplitudes[18]. This phenomenon, which is not yet understood in full detail, gives rise to spurious rf signals in the photodetector that interfere with and can bury weak absorption signals from a sample.

A number of methods have been devised to overcome the RAM problem. Some approaches use external techniques such as special polarization schemes [19] or optical nulling of RAM in a double-beam configuration[20], whereas another approach is based on an additional internal modulation of the absorption lines under consideration, hence the name, double modulation. An example of the latter principle is the photochemical modulation of the Schuler absorption bands of ND_4 in conjunction with FMS[21]. Very recently, an internal Stark effect modulation of the absorption lines was used in an FM experiment to detect transient holes and SFS in the R_{1m} transition band of Cr^{3+} ions in alexandrite[5]. In our single-molecule detection (SMD) experiment, we also used either of two internal secondary modulation techniques for suppressing RAM. The first method (FM Stark) involves a Stark effect modulation similar to that described in Ref. 5, whereas the second one (FM US) uses ultrasound of different polarizations and frequencies to periodically shift the absorption lines in the sample. Previously, ultrasonic modulation (without FMS) was applied to the sensitive detection of shallow persistent spectral holes [22,23].

B. Experimental Configuration

Because of the difficulty of single-molecule detection, the experimental apparatus will be described thoroughly. The optical set-up and the common electronic components of our apparatus are shown in Figure 3. The radiation from an actively stabilized, tunable single-mode cw dye laser DL (Coherent 599-21) with an effective linewidth of about 2-3 MHz was first passed through an amplitude stabilizer AS (Cambridge Research LS-100) for reduction of low-frequency power fluctuations. This was necessary because actual signals and or RAM shift the low-frequency laser fluctuations up to ω_m, even though in the absence of any signal or RAM the background in FMS is near the shot-noise limit. Next, the beam was focussed through the electro-optic phase modulator EO (Crystal Technology Model 6100, containing three $LiTaO_3$ crystals). The radio frequency used to drive the phase modulator was generated by a precision rf oscillator RFI (Marconi Instruments 2019A) whose output was split by a two-way, 0° power splitter PS. One output port of the splitter was connected to the phase modulator through an rf phase shifter ϕ and a tunable rf power amplifier A (Hewlett-Packard 230B), while the other port provided the local-oscillator signal LO1 for the mixer in the first demodulation step (see below). The rf frequencies used ranged between 50 and 100 MHz, and the FM modulation index was adjusted to approximately 0.8.

From the phase modulator, the laser light was bounced off a confocal Fabry-Perot etalon FP1 (Tropel 240 with 1.5 GHz FSR). The narrow absorption fringes of this etalon provided a strong FM signal which was used for optimizing the alignment of the photodetector PD1 and for measuring the detection sensitivity of the apparatus. During the actual SMD measurements, the resonances of the etalon were placed outside the 0.5 or 1 GHz wide laser scan range, and the etalon simply acted as a mirror. A Fresnel rhomb polarization rotator PR after the etalon provided the possibility of rotating the polarization axis of the linearly polarized light in any direction for matching the transition-dipole axis of the aligned dye molecules in the sample. At this point, a beam splitter BS split off a reference beam which

was necessary for correct adjustment of the rf phase (see below). The sample beam entered the cryostat and was focused onto the sample S, which was kept at 1.5K in superfluid helium.

In the early stage of the SMD experiments, we used a high-quality achromatic doublet lens with 75 mm focal length located outside the cryostat for focussing. However, with this method we observed single-molecule signals which changed on the time scale of a few minutes and therefore exhibited poor reproducibility. We believe that the sample holder mounted at the lower end of a stainless-steel rod inside the cryostat was subject to slow creeping motion resulting from thermal expansion as the level of the superfluid helium in the sample chamber went down. Therefore, a single molecule originally in focus in the micron-sized focal volume wandered out of the laser focus within a few minutes. We solved this problem by replacing the focussing achromat lens with a small 0.47 numerical aperture (NA) three-element lens of 4.2 mm focal length (Olympus AV4647-3) designed for application in optical storage devices, which was mounted on the sample holder inside the superfluid helium. In this case, thermal motion caused the focussing lens to move together with the sample, so that the motion of the focal spot relative to the sample was only of second order. Using this configuration it was possible to observe a single molecule for more than an hour. Since the focal length of the lens slightly changed between room temperature and 1.5K, we found it favorable to have the possibility of adjusting the distance between lens and sample inside the cryostat. We achieved this by mounting the lens on a strip of thin stainless-steel shim stock, one end of which was rigidly connected to the sample holder, while the other free end carried a small CoSm magnet. A small coil was mounted on the sample holder adjacent to the magnet. By adjusting the current through the coil it was possible to move the lens over a distance of roughly 2 mm in the superfluid helium. The light transmitted through the sample was focussed onto a fast Si avalanche photodiode (RCA C30950F with integral preamplifier).

The light beam reflected off the first beam splitter was used to generate a reference FM signal with the same rf phase as that of spectral features in the sample. The reference beam

was bounced off another confocal Fabry-Perot etalon FPIR (same model as FPD, and the outgoing beam was directed to a second identical avalanche photodetector PDIR by means of a second beam splitter. Care was taken to match the light paths from the first beam splitter to the sample and to FPIR as well as from either of these points to the respective photodetectors to within a small fraction of the rf wavelength. In addition, the detection electronics behind the photodetectors, which is described in the following paragraph, was made as identical as possible up to the first-stage mixers. In this way, by observing the strong FM signal from the resonance fringes of FPIR, it was possible to easily adjust the desired phase of the rf used for driving the FO modulator[21]. This was crucial for recognizing and interpreting the line shape of the single molecule signals (see below). After adjustment of the rf phase, the light path to FPIR was blocked between the two beam splitters in order to rule out any possible influence of the back-reflection from the etalon on the light in the sample path. In both paths, the light intensity could be adjusted independently by using combinations of fixed and variable neutral density attenuators VA.

The detection electronics used in the FM Stark and FM US experiments is depicted in Figs. 4(a) and 4(b), respectively. Up to the first stage mixers M1, the set-up was identical in both cases. The signals from the two photodetectors were first fed through -20dB directional couplers DC. The -20dB-port of the coupler in the sample path was connected to an rf spectrum analyzer SA (HP 8590A) for diagnostics, whereas in the reference path the -20dB-port was terminated in a 50Ω load T. The spectrum analyzer allowed observation of the intermodulation signals at sums and differences between the rf modulating frequency and the secondary internal modulation frequency. This signal allowed optimization of the position of the focus of the small lens in the cryostat (see below). After the directional couplers the signals passed through 50 MHz high-pass filters HPF to suppress low-frequency signals that might arise from overall amplitude variations of the light in the sample due to the secondary modulation. Slight periodic changes in the sample transmission could arise from electrostriction effects in the case of Stark modulation and from compression and rarefaction

in the case of the FS experiment. The filtered signals were fed into the rf ports of matched double-balanced mixers M1 (Mini-Circuits ZFM-2) which performed the first-stage demodulation (with respect to the FM). The local-oscillator signal LO1 for these mixers was provided by the Marconi 2019A generator (see above) and split into equal parts by a two-way, 0° power splitter PS. The intermediate-frequency port of the mixer in the reference path was connected to a custom-built, low-noise post-mixer-preamplifier PMPA #3, and the amplified FM signal of the resonance fringe from etalon FPIR was observed on an oscilloscope O. This signal was used to adjust the rf phase. The further processing of the output of the mixer in the sample path was different for the FM/Stark and the FM-US method.

For the FM Stark scheme, the sample was mounted between two sapphire plates coated with transparent but conducting indium-tin-oxide (ITO) coatings on their inner surfaces. A custom-built AC HV power supply provided bipolar oscillating Stark voltages of up to 1600V pk-pk at frequencies between 2 kHz and 5 kHz. We used two different waveforms for this voltage, namely either a sinusoid or a bipolar square wave (see Fig. 4a). Since pentacene in a *p*-terphenyl host crystal exhibits a quadratic Stark effect[25], the second-step demodulation of the signal (with respect to the Stark field) was performed with a lock-in amplifier LIA (Ithaco 393A) at twice the modulating frequency. Therefore, the output of the mixer M1 in the sample path was first amplified using another home-built post-mixer preamplifier (PMPA #2) and fed into the lock-in. The demodulated signal was finally stored in a digital oscilloscope (a Data Precision 6100 waveform analyzer with a 100 kHz, 14 bit digitizing plugin). Parallel to the demodulation in the lock-in, the output of PMPA #2 was bandpass-filtered (0.1-300 Hz) and fed into an oscilloscope O. In this way it was possible to observe the strong SFS at the center of the inhomogeneous line in simple FM without secondary modulation.

In the FM/US experiment, the sample was bonded to a PZT or quartz transducer for application of either longitudinal or shear waves; the eigenfrequencies of the transducers ranged between 2 MHz and 5 MHz. The transducers were driven by the output of a synthesized rf generator RF2A (Hewlett-Packard 3325A) (see Fig. 4(b)). In this case, the absorption lines were shifted linearly with the applied stress field, and the second-step demodulation had to be performed at the modulating frequency with another rf mixer. Therefore, the output of the first-stage mixer M1 was split by a resistive power splitter RPS, one of whose output signals was narrow-band amplified around the US frequency by a chain of bandpass filters BPF and an rf signal amplifier A (Trontech W50K). In the case depicted in Fig. 4(b) an ultrasonic frequency of 2 MHz was utilized. The amplified signal was fed into the rf port of the second-stage mixer M2 (Mini-Circuits ZFM-3), whose local-oscillator signal was provided by a second rf generator RF2 which was phase-locked to RF2A. The output of M2 was amplified by PMPA #2, bandpass-filtered and stored in the digital oscilloscope DO. The second output signal of the resistive power splitter was directly amplified by PMPA #1, bandpass-filtered and fed into an oscilloscope O for the observation of strong SFS signals in simple FM.

For recording SFS or SMD, the laser was scanned continuously over a frequency interval between 0.5 and 1 GHz in width, and the scans were averaged in the digital waveform analyzer DO. One final trace was obtained by averaging usually 128 or 512 single scans. In most of the experiments the laser scan rate was adjusted to the fastest possible value of 0.25 s/scan. Thus the final detection bandwidth was controlled by the final bandpass filter or the lock-in, modified by the number of averages.

C. Sample Characteristics

The low-temperature electronic absorption spectrum of pentacene in *p*-terphenyl is known to consist of four inhomogeneous $|S_1> \leftarrow |S_0>$ site origins of almost equal width and intensity, corresponding to pentacene substitution of each of the four inequivalent

p-terphenyl molecules in the low-temperature unit cell [25,26]. Generally, these inhomogeneous absorption lines are referred to as O_1 to O_4 in the order of increasing transition energy. The two longest-wavelength origins O_1 and O_2 are centered around 592.32 nm and 592.18 nm, respectively, whereas the transition wavelengths of O_3 and O_4 are about 4 nm shorter. Since the inhomogeneous widths of all four bands are $\simeq$ 40 GHz (0.05 nm), O_1 and O_2 have a slight overlap, but are well separated from the next origin O_3. For this reason, single-molecule spectra could only be recorded at the long-wavelength edge of O_1 and at the short-wavelength edge of O_2, but not in between them. No attempt at SMD was made in O_3 and O_4, since these two lines showed only weak and broad SFS features in a previous study[4], probably due to higher ISC rates and longer triplet lifetimes.

Sublimed pentacene and zone-refined *p*-terphenyl were used for sample preparation. First, the dopant and the host were mixed and pre-melted to achieve good dispersion of the dopant. Single crystals were grown from the doped mixtures using the Bridgman technique. The actual samples were cleaved from the Bridgman boule and had thicknesses of 100-200 μm. For single-molecule detection, the dye concentration was chosen between 2×10^{-7} and 1×10^{-6} mole/mole. In order to compare the line shapes obtained in SMD to those of similar but stronger signals, we also burned persistent spectral holes and detected them both in simple FM and in FM/Stark double modulation. Since the hole-burning efficiency is extremely low in this system [3,4], we used samples of higher concentrations (typically 2.5×10^{-6} mole/mole) for the hole-burning studies.

III. Theory

A. Line Shape of Single-Molecule Signal in Double Modulation

In this section, we present a simple theory for the detected shape of a Lorentzian absorption line in our double-modulation experiment. The calculation is applicable to

single-molecule lines as well as to spectral holes, as long as the modulation index is less than unity. In order to generate explicit expressions, we specifically consider the case of FM-US double modulation with a linear dependence of the molecular line shift on the ultrasonic field. The extension of the calculation to the cases of linear or quadratic Stark effect modulation is straightforward, and the resultant line shapes are identical in all these cases, as long as the line shift is less than the homogeneous width.

We begin with the detector photocurrent in a simple FM experiment. According to well-known FM theory[17], the detector photocurrent I_d is given by

$$I_d \propto E_0^2 e^{-2\delta_0}[1 + (\delta_- - \delta_+)M \cos \omega_m t + (\phi_+ + \phi_- - 2\phi_0)M \sin \omega_m t] . \qquad (3)$$

In this equation, E_0 and M are the electric field strength and the FM modulation index, ω_m is the modulation frequency, and δ_0 , δ , δ_+ (ϕ_0, ϕ , ϕ_+) are the electric field absorption (dispersion) signals of the sample at the frequencies of the carrier and the lower and upper sideband, respectively. Equation (3) is valid in the limit of small modulation index and small differences in the absorption and dispersion values at the three frequencies: M, $|\delta_0 - \delta_+|$, $|\delta_0 - \delta|$, $|\phi_0 - \phi_+|$, $|\phi_0 - \phi| << 1$. The effect of the first-stage mixer is to multiply I_d by the local oscillator LO1 which oscillates as $\cos(\omega_m t + \theta)$, where θ is the rf phase difference between I_d and the local oscillator at the position of the mixer. By proper low-pass filtering, we need consider only the "baseband" signal at the IF port of the mixer, given by

$$I_1 = \frac{1}{2} M E_0^2 e^{-2\delta_0}[(\delta_- - \delta_+) \cos \theta - (\phi_+ + \phi_- - 2\phi_0) \sin \theta] . \qquad (4)$$

By proper choice of θ it is possible to pick either the pure absorption ("S_1"; $\theta = 0$) or the pure dispersion ("S_2"; $\theta = \pi/2$) signal of the sample[24].

In the following we calculate the double-modulation line shape for a Lorentzian absorption line with height δ_{max}, full-width at half-maximum (FWHM) 2Γ, and center frequency $\bar{\omega}$, which has the following form:

$$\delta(\omega) = \delta_{max}\pi\Gamma L_\Gamma(\omega - \overline{\omega}) \tag{5a}$$

$$\phi(\omega) = \delta_{max}\pi(\omega - \overline{\omega})L_\Gamma(\omega - \overline{\omega}) \tag{5b}$$

with the normalized Lorentzian defined by

$$L_\Gamma(\omega - \overline{\omega}) = (\Gamma/\pi)\left[(\omega - \overline{\omega})^2 + \Gamma^2\right]^{-1}. \tag{6}$$

We assume that the secondary US modulation causes a sinusoidal oscillation of the center frequency $\overline{\omega}$ at frequency ω_Λ. Then, for instance, the absorption signal at the lower FM sideband is given by

$$\delta_-(t) = \delta_{max}\pi\Gamma L_\Gamma[\omega_c - \omega_m - \overline{\omega}(1 + m\cos\omega_\Lambda t)], \tag{7}$$

with ω_c being the frequency of the (light) carrier. We restrict ourselves to the case that the amplitude m of the oscillation is small compared to the linewidth and, hence, we perform a Taylor expansion of Eq. (7) up to first order in m,

$$\delta_-(t) \approx \delta_-^0 - \delta_{max}\pi\Gamma\overline{\omega}m\cos(\omega_\Lambda t)L'_\Gamma(\omega_c - \omega_m - \overline{\omega}), \tag{8}$$

where the prime denotes the derivative of the Lorentzian with respect to its argument and $\delta_-^0 \equiv \delta_-(m = 0)$. A similar expansion can be done for the upper sideband absorption signal and for all three dispersion terms. In the pure S_I phase ($\theta = 0$), the signal at the I port of the first mixer oscillating at ω_Λ is then given by

$$\begin{aligned} I_I(\theta = 0) = \frac{1}{2}ME_0^2e^{-2\delta_0}\{(\delta_-^0 - \delta_+^0) - \delta_{max}\pi\Gamma\overline{\omega}m\cos(\omega_\Lambda t) \\ [L'_\Gamma(\omega_c - \omega_m - \overline{\omega}) - L'_\Gamma(\omega_c + \omega_m - \overline{\omega})]\}. \end{aligned} \tag{9}$$

In the second-stage mixer, this function is multiplied by the US local oscillator, $\cos(\omega_A t + \psi)$. Picking again only the slowly varying "baseband" term leads to the following form of the double-modulation signal in the absorption (S_1) phase:

$$I_2(\theta = 0) = \frac{1}{2} mME_0^2 \delta_{max} \Gamma^2 \overline{\omega} e^{-2\delta_0} \cos\psi \left\{ \frac{\omega_c + \omega_m - \overline{\omega}}{\left[(\omega_c + \omega_m - \overline{\omega})^2 + \Gamma^2\right]^2} - \frac{\omega_c - \omega_m - \overline{\omega}}{\left[(\omega_c - \omega_m - \overline{\omega})^2 + \Gamma^2\right]^2} \right\}. \tag{10}$$

In order to obtain maximum signal amplitude, the phase ψ of the local oscillator at the second-stage mixer must be properly adjusted; however, in contrast to the situation at the first-stage mixer, a detuning of ψ from the optimal value only causes a decrease in signal (or a sign change) and does not give rise to a change of the line shape.

In an analogous way to the absorption, the dispersion or S_2 signal at the output of the second mixer can be calculated. We start out by picking $\theta = \frac{\pi}{2}$ in Eq. (4) and inserting approximations for the time-dependent ϕ values similar to Eq. (8). The "baseband" signal at the output of the second mixer becomes

$$I_2\left(\theta = \frac{\pi}{2}\right) = \frac{1}{4} mME_0^2 \delta_{max} \Gamma \overline{\omega} e^{-2\delta_0} \cos\psi \left\{ \frac{2\left[(\omega_c - \overline{\omega})^2 - \Gamma^2\right]}{\left[(\omega_c - \overline{\omega})^2 + \Gamma^2\right]^2} - \frac{(\omega_c + \omega_m - \overline{\omega})^2 - \Gamma^2}{\left[(\omega_c + \omega_m - \overline{\omega}^2 + \Gamma^{-2}\right]^2} - \frac{(\omega_c - \omega_m - \overline{\omega})^2 - \Gamma^2}{\left[(\omega_c - \omega_m - \overline{\omega})^2 + \Gamma^2\right]^2} \right\}. \tag{11}$$

Plots of Eqs. (10) and (11) for two different linewidths Γ as well as the corresponding signal shapes in simple FM, for comparison, are shown in Fig. 5. The characteristic features of the double modulation signal in S_1 phase [Eq. (10), Figs. 5(c), 5(d)] are a large positive and a large negative slope, centered around the real position $\overline{\omega}$ of the absorption line and separated by twice the FM modulating frequency ω_m. This "W"-like shape may change into an "M", if either of the phases θ or ψ is shifted by π. The dispersion signal [Eq. (11), Figs. 5(g),

5(h)], on the other hand, is characterized by a large positive peak at $\overline{\omega}$ and two smaller negative peaks (of half the amplitude of the central peak) at $\overline{\omega} \pm \omega_m$. Again, the overall sign of this line shape may change, depending on θ and ψ. The amplitude of the dispersion signal is bigger than the absorption signal, the quotient between the maximum values being

$$\frac{I_{2,max}\left(\theta = \frac{\pi}{2}\right)}{I_{2,max}(\theta = 0)} = \frac{16}{3\sqrt{3}} \approx 3.1 . \tag{12}$$

Nevertheless, we found it more favorable to choose the S_1 phase in our SMD experiments, since the "W" (or "M") line shape is simpler and easier to recognize, especially in a background of other out-of-focus weak single-molecule signals (see below).

B. Estimated Amplitude of Single-Molecule Signals

Generally, the (power) absorbance of a center with peak cross section σ in a light beam of area A is given by

$$(\Delta\alpha)L = \sigma/A . \tag{13}$$

Therefore, the detection of single molecules should be easiest for molecules with strong absorption lines (large σ) and a tightly focussed laser beam (small A). For pentacene in *p*-terphenyl the transition dipole moment of the purely electronic $|S_1> \leftarrow |S_0>$ transition in the O_1 site was measured to be 0.71D [27], and the 1.8K linewidth (FWHM) of the O_1 and O_2 sites was determined to be 7.8 MHz and 7.3 MHz, respectively[28]. This results in values for the peak absorption cross section σ of 9.3×10^{-12} cm^2 and 9.9×10^{-12} cm^2, using a standard formula given by Hilborn [29]. From measurements of the light power transmitted through small pinholes, the focal waist diameter of our laser beam was estimated to be roughly 3 μm. Using this value and $\sigma = 9.3 \times 10^{-12}$ cm^2 for the O_1 site, we obtain a theoretical signal amplitude of $(\Delta\alpha)L = 1.3 \times 10^{-4}$.

In this calculation, it was assumed that there is no power broadening of the molecular absorption line. In a tightly focussed laser spot, on the other hand, it is relatively easy to achieve the conditions of power broadening, especially in optical three-level systems which have a long-lived bottleneck such as the lowest triplet state $|T_1>$ in between $|S_1>$ and $|S_0>$. According to Ref. 30, the light-power-dependent linewidth of an optical three-level system is given by

$$\Delta\nu_h = \frac{\Gamma}{\pi} = \frac{1}{\pi T_2}\sqrt{1 + \hat{K}^2 T_2^2} \tag{14}$$

where T_2 is the phase relaxation time and $\hat{K}^2 = \chi^2(2 + \Lambda)/2T_2K_2$. In the latter expression, χ denotes the (light-dependent) Rabi frequency, $\Lambda = k_{23}/k_{21}$ is the quotient between the transition rates into and out of the bottleneck state, and $K_2 = k_{21} + k_{23}$ is the total decay rate of the excited singlet state $|S_1>$ (which is equal to the inverse fluorescence lifetime). The critical light intensity I_{sat} at which power broadening begins can be calculated by setting $\hat{K}^2T_2^2 = 1$. This leads to the expression:

$$I_{sat,3LS} = \varepsilon_0 c_0 h^2 \frac{K_2}{\mu_{12}^2(2 + \Lambda)T_2} . \tag{15}$$

For pentacene in *p*-terphenyl, we insert the values [28,31] $K_2 = 4.26 \times 10^7\ s^{-1}$, $\mu_{12}^2(2 + \Lambda) = 4.3 \times 10^{-59}\ C^2\ m^2$, $T_2 = 41$ ns, and we obtain the saturation intensity $I_{sat,3LS} = 71\ mW/cm^2$.

If the bottleneck state is not taken into account, the saturation intensity for a two-level system reads [30]

$$I_{sat,2LS} = \varepsilon_0 c_0 h^2 \frac{1}{2\mu_{12}^2 T_1 T_2} , \tag{16}$$

This formula is obtained from Eq. (15) by replacing K_2 by the inverse fluorescence lifetime T_1^{-1} and setting $\Lambda = 0$. In the case of pentacene at 1.5 K the value is $I_{sat,2LS} = 1.1\ W/cm^2$.

In order to obtain an acceptable signal-to-noise ratio, we performed most of our measurements with a light power of 0.3 μW. At this value, the total intensity in the 3 μm diameter focal spot is 4.2 W/cm^2 (i.e., 0.85 W/cm^2 in one sideband). Since the absorption cross section decreases in the case of saturation as [32]

$$\sigma(I) = \sigma(I \to 0)\frac{1}{1 + I/I_{sat}} , \tag{17}$$

we would expect a peak σ value of only 7.2×10^{-13} cm^2, if the molecule behaved as a usual three-level system. An absorption line this weak is hardly observable even with our ultrasensitive apparatus. Our experimental single-molecule spectra, on the other hand, correspond to σ values on the order of 4.9×10^{-12} cm^2 (see Section IV), which is closer to the theoretical value if the (higher) two-level saturation intensity is inserted in Eq. (17). Although the absolute measurement of absorption strength is very difficult, this comparison provides evidence for the possibility that the singlet-triplet transition rates of molecules in highly strained sites (which absorb far out in the wings of the absorption line) are different from those in equilibrium sites near the center of the inhomogeneous line.

In the above calculation we used quantities such as the phase relaxation time and the transition rates between the energy levels, which are usually defined (and measured) for an ensemble of many molecules. Therefore, the question arises whether or not these quantities are meaningful in the case of one single absorber in resonance. A crucial feature of our experimental conditions is that we do not probe single quantum jumps in the molecule but perform the experiment under conditions where many transitions between its energy levels occur during the observation time. Therefore, time-averaged measurements on a single absorber are meaningful and (by the ergodic theorem) would be expected to provide the same information as an ensemble of many molecules in essentially identical surroundings.

IV. RESULTS AND DISCUSSION

A. FM/Stark Measurements

Persistent Spectral Holes

In order to compare the theoretical line shapes of an FM/double modulation experiment to real experimental waveforms provided by a strong Lorentzian spectral feature in the sample, we performed measurements on persistent holes burnt near the center of the O_1 band of a more heavily doped (2.5×10^{-6} mole/mole) pentacene/*p*-terphenyl mixed crystal. Such studies also verified that our external electric field strength values were sufficient to shift the absorption lines by a noticeable fraction of the homogeneous linewidth. The pentacene/*p*-terphenyl system exhibits persistent spectral hole-burning although the efficiency is extremely low[3,4]. The mechanism is not yet fully understood, but since the holes are observed to decay on a time scale of several minutes, we suggest that the mechanism involves a flip of the central phenyl ring of a nearby *p*-terphenyl molecule from its normally cocked position to another metastable orientation. In effect, certain pentacene molecules may be coupled to a nearby two-level system. For the hole-burning experiments, we took the small optical storage lens out of the cryostat and adjusted the diameter of the laser beam hitting the sample to $\simeq$ 1 mm in order to reduce the SFS signal and obtain a smoother baseline[4].

Figure 6 shows four traces of a hole in simple FM spectroscopy (S_1 phase), which was burnt near the center of the O_1 line at 592.328 nm. To burn the hole, we irradiated with a light power of 30 μW for 10 minutes with no phase modulation of the laser light and no electric field applied to the sample. For recording the spectra, the light power was reduced to 3 μW, and 64 scans were averaged. Trace (a) shows the hole immediately after burning with no voltage applied. The signal clearly shows the typical S_1 FM line shape of a Lorentzian spectral feature[24]. The linewidth, however, is much larger than twice the homogeneous linewidth of 15.6 MHz although the light intensity in the defocused laser spot

was only about 4 mW/cm^2 during burning which is well below the saturation limit (see Section III). The reason may be due to the nonphotochemical nature of the hole-burning mechanism or perhaps a slight heating of the sample due to the high total light energy required.

The traces (b), (c), and (d) in Fig. 6 show subsequent scans over the same hole with dc fields of 28 kV/cm, 45 kV/cm, and 0 kV/cm, respectively, applied. Trace (d) was taken at the end of this series. The comparison between (a) and (d) shows that there is a substantial decrease in hole area within a few minutes, corresponding to a back-reaction of the photoproduct. In traces (b) and (c) which were recorded with electric dc fields applied, the hole is slightly shifted to lower frequencies and, moreover, it is substantially broadened. Both the red shift and the broadening are reversible and disappear when the field is turned off (see trace (d)). For pentacene in *p*-terphenyl, the Stark shifts were measured previously [33] and red-shift values of 1.40×10^{-6} cm^{-1}, 4.38×10^{-6} cm^{-1}, and 5.33×10^{-6} cm^{-1} were reported for an electric field strength of 1 kV/cm applied along the crystallographic a, b, and c axis, respectively. At a field strength of 45 kV/cm, this would correspond to a shift between 85 MHz and 320 MHz, depending on the crystal orientation. The actual shift measured, on the other hand, is only $\simeq$ 100 MHz. Thus, it seems that the field strength experienced by the dye molecules is somewhat smaller than expected, probably due to screening effects caused by space or surface charges in the sample [33,34]. Also the distinct broadening of the hole indicates the presence of charge carriers giving rise to different amounts of screening of the E field at the locations of different molecules. In spite of this problem, the data in Fig. 6 indicate that field strengths of a few tens of kV/cm are sufficient to shift the pentacene absorption lines by a sizeable amount and, therefore, that the FM/Stark double modulation approach should be suitable to detect single-molecule spectra.

Figure 7 shows spectra of persistent holes taken in simple FM and FM/Stark double modulation under various conditions. Because of the rapid decay of the hole area, the data

were taken on different holes which were all burnt near the center of the O_1 band under the same conditions as the hole shown in Fig. 6. The light power used for probing the hole spectra was 3 μW in all cases. Since different periods of time elapsed between burning and scanning the holes, their absolute amplitudes are not comparable, which, however, does not affect the line shapes of the spectra in any way.

Trace (a) in Fig. 7 shows a hole in simple FM detection with no electric field applied to the sample. This spectrum was taken under the same conditions as in Fig. 6(a) and has been added here for comparison. The four lower traces in Fig. 7 show hole spectra recorded in FM/Stark double modulation. In each case a bipolar sinusoidal E field at 5 kHz with peak value 28 kV/cm was applied to the sample, and lock-in detection at twice the modulating frequency (10 kHz) was performed (see Fig. 4(a)) with a time constant of 1.25 ms. In traces (b) and (c) the phase of the rf local oscillator was adjusted to give the pure S_1 component of the signal, whereas in traces (d) and (e) the pure S_2 phase was selected. The value of $\omega_m/2\pi$ was 75 MHz in the case of (b) and (d) and 90 MHz in (c) and (e), respectively.

The comparison of these four double-modulation spectra of persistent holes with the corresponding theoretical line shapes (Fig. 5(c) and (g) for a broader Lorentzian) shows that the theory properly describes the salient features both in the S_1 and the S_2 phase (apart from a trivial sign reversal in S_2). In S_1, the experimental spectra are characterized by a large negative slope and a large positive slope separated by exactly twice the rf modulating frequency. A change of the rf frequency causes this "W" shape to expand (or contract) accordingly. A slight asymmetry of the experimental hole signal, which especially appears in trace 7(b) may be due to a small detuning of the rf phase from exactly S_1 ; also the underlying SFS signal may give rise to a marginal distortion. In the S_2 phase, the basic features are a strong negative peak which is bracketed by two positive peaks of half its amplitude. The distance between the positive peaks is again given by twice the radio frequency, so that the whole structure expands as $\omega_m/2\pi$ is changed from 75 to 90 MHz.

Single-Molecule Data

In order to find appropriate spectral positions for observing single-molecule signals, we first measured the variations of the SFS amplitude across the inhomogeneous O_1 and O_2 bands of pentacene in *p*-terphenyl using the FM/Stark method. The results are shown in Fig. 8. The circles in Fig. 8 represent the mean-square values of SFS as measured in scans over 0.5 GHz wide spectral regions. The background mean-square noise level (as measured far away from the absorption lines) has been subtracted from the raw data. Together with the SFS data, regular absorption spectra of the O_1 and O_2 bands are plotted (smooth curves) which were recorded on a higher-concentration sample ($\approx 2.5 \times 10^{-6}$ mole/mole) with a scanning monochromator. The root-mean-square (RMS) values of the SFS are proportional to the fluctuations in the absorption coefficient and therefore, to the fluctuations of the number N_H of absorption lines per homogeneous linewidth. According to the fundamental laws of statistics of independent additive quantities, these fluctuations vary as the square root of the mean value $\overline{N}_H$ in the limit $\overline{N}_H >> 1$. As a consequence, the mean-square (MS) of the SFS spectra should scale with $\overline{N}_H$ and, thus, with the mean absorption coefficient that is measured by the monochromator. These relations are summarized in Eqs. (18a) and (18b).

$$RMS_{SFS} \sim (\Delta\alpha)L \sim \Delta N_H \sim \sqrt{\overline{N}_H} \tag{18a}$$

$$MS_{SFS} \sim \overline{N}_H \sim \alpha_0 L . \tag{18b}$$

Figure 8 shows that there is indeed a good correlation between the MS values of the SFS and the average absorption coefficient. The scatter in the SFS mean-square values are to be expected since the SFS, being a statistical quantity, is itself subject to statistical fluctuations. The arrows indicate typical spectral positions where we observed single-molecule spectra in our low-concentration samples ($\approx 2.5 \times 10^{-7}$ mole/mole). These wavelengths are very far away from the peaks of the inhomogeneous bands, if one considers the shapes of

the bands as strictly Gaussian. At a dye concentration of 2.5×10^{-7} mole/mole, the $\bar{N}_{II}$ values at the center of each band are estimated to be in the range $10^3 - 10^4$ for our focal volume. Using a width of the inhomogeneous distribution in the O_1 band of 42 GHz [26] and assuming a strictly Gaussian decrease of $\bar{N}_{II}$ towards the wings of the band, one would predict that $\bar{N}_{II} \approx 10^{-8} - 10^{-7}$ at the position of the right arrow (592.457 nm). It is obvious that there are slowly-decaying tails on the inhomogeneous lines, which extend out much farther than predicted by the Gaussian model. Probably these sites correspond to dye molecules near major lattice imperfections such as point defects and dislocations and are, therefore, highly strained and shifted by a large amount from the equilibrium position.

Single-molecule spectra recorded at the wavelength of the right arrow in Fig. 8 and obtained with the FM Stark technique are shown in Fig. 9. The first trace in Fig. 9 is a calculated double-modulation spectrum which has been added for comparison. Trace (b) in Fig. 9 shows an overlay of eight experimental scans over the same spectral region at 592.455 nm which contain a strong single-molecule signal near the center of the scan. Each of these traces was obtained by averaging the data of 512 single laser scans. The fiducial bar above the strong feature marks a distance of $2\,\nu_m = 150$ MHz. The shape of the strong single-molecule signal is very similar to the theoretical line shape (trace (a)) and also to the signals of persistent spectral holes probed with the double-modulation method (Figs. 7(b) and (c)). However, in the center the measured lineshape shows a peak which is stronger than expected. This slight deviation from theory is most probably due to an admixture of a small amount of the S_2 phase. In addition to the strong feature, the traces of Fig. 9(b) contain smaller repeatable signals, especially at the left edge. These are presumably caused by other molecules which are located away from the laser focus, where the cross-section of the beam is larger than at the waist and, according to Eq. (13), the signal amplitude is correspondingly lower. In trace (c) the average of the eight scans has been calculated and the contribution of the S_2 phase has been subtracted so as to obtain a least-squares fit between the strong central feature and the theoretical line shape (thick line overlaid). The latter was obtained

using Eq. (10). The fit is very satisfactory; especially the most pronounced features – the large negative slope and the large positive slope separated by $2\nu_m$ – are well-reproduced by the fit.

The two traces in Figs. 9(d) and (e) show double-modulation spectra taken very far off the inhomogeneous band on the doped sample and at the center of the O_1 band on an undoped *p*-terphenyl crystal, respectively. In both cases, no absorption lines of pentacene molecules are expected to be present. The signals therefore reflect the noise level of our double-modulation technique, which is composed of shot noise and a certain amount of avalanche noise of the photodetector. The contribution of the avalanche noise is unavoidable, since a detection light power level of 0.3 μW is too high for the use of a photomultiplier and not high enough for the shot-noise-limited operation of a regular photodiode with 50 Ω load. For the sake of comparison with the single-molecule data, two overlaid SFS spectra recorded at the center of the O_2 line for the doped sample have been added in Fig. 9(f). In contrast to the former, these spectra are composed of signals from many molecular absorption lines and, as a consequence, show strong repeatable features all over the scan range.

We observed single-molecule signals similar to those in Fig. 9 on several occasions with several different samples; however, it was not possible to reliably obtain SMD spectra each day with the FM/Stark technique. The problem was most probably due to an electrical phenomenon well-known in organic crystals[33,34]: the injection of charge carriers from the electrodes into the interior of the crystals. The injected charges give rise to strong internal electric fields which add to the externally applied field and, moreover, may vary in an unpredictable manner as part of the charges move around under the action of the external AC field. Since the charges are expected to be trapped in different surroundings, their motions should have different amplitudes and different phase shifts with respect to the driving field. Strong evidence for the presence of injected charge carriers comes from the data shown

in Fig. 10. Part (a) contains 8 spectra recorded at the blue edge of the O_2 band at 592.057 nm. The concentration of the sample was 2.5×10^{-7} mole/mole and the radio frequency was $\nu_m = 50$ MHz. A repeatable "W"-like single-molecule signal is clearly visible around a relative laser frequency of 230 MHz. At the left and right edges of the scan range additional repeatable features are located which may be due to other molecules. Trace (b) shows the average of the eight scans contained in (a). In this case, the internal Stark modulation was produced by an electric field in the form of a bipolar square wave at 5 kHz. The remarkable point in the experimental conditions used for recording these spectra, however, was that the second-stage demodulation in the lock-in amplifier was performed at the modulation frequency ω_A rather than at $2\,\omega_A$. Therefore, the lock-in was probing line shifts due to the *linear* Stark effect. Since isolated pentacene, due to its center of symmetry, does not exhibit an intrinsic linear Stark effect, neither in the $|S_0>$ nor in the $|S_1>$ state, this observation strongly indicates that an injected charge carrier is located near the molecule, inducing permanent dipole moments via its Coulomb field. It is unlikely that a polar impurity molecule other than pentacene gives rise to this SMD signal for two reasons: First, the signals were observed in the blue tail of the characteristic O_2 site origin for pentacene in *p*-terphenyl. Far away from the inhomogeneous origins no such spectra were observed, as traces (c) show which were recorded at 593.071 nm. The second reason is that an impurity molecule with a much broader absorption line than pentacene cannot be observed with the FM technique, since the sensitivity of the FM method is restricted to spectral features with widths on the order of or narrower than ν_m (see Section II).

It is in principle possible that the electric dipole moments of the pentacene molecule responsible for this linear Stark effect are induced by an ionic or strongly polar impurity molecule nearby rather than an isolated injected charge carrier. However, this also seems unlikely considering the large SFS signal at the center of the O_2 line that was observed in the same sample with linear Stark-effect detection (Fig. 10(d)). This specific sample was cleaved from a Bridgman boule that was grown from extensively zone-refined *p*-terphenyl and

sublimed pentacene and that provided several other samples which showed only very weak SFS signals near the centers of the pentacene absorption lines using the linear Stark effect. The presence of a large amount of impurity molecules other than pentacene can therefore be ruled out. The linear Stark effect giving rise to the data in Fig. 10 seems indeed to be due to the injection of charge carriers, which in this specific sample may have been especially numerous due to good contacts between the sample and the electrodes and to the extended period of time in which the sample was exposed to large electric fields. These experimental findings may lead to several interesting applications of SMD, namely the study of single charge carrier traps in organic materials and of local environments with lowered symmetry due to nearby charges. Previously a different optical method for the detection of injected charges in a polymeric sample was reported [35] which was based on persistent spectral hole-burning; however, it measured the macroscopic electric field generated in the sample by the injected charges and was therefore insensitive to local effects.

B. FM/Ultrasound Measurements

The study of the local surroundings of single injected charge carriers may become an interesting field; however, for the detection and spectroscopy of single dye molecules the effect of charge injection and motion is undesirable, since it gives rise to poor reproducibility of the Stark shifts. In order to overcome this problem and to provide confirmation of our single-molecule results with a distinct technique, we used a different secondary modulation of the absorption lines, namely the application of time-varying stress fields with ultrasound. The corresponding demodulation was performed at the ultrasonic frequency using a second rf mixer (see Fig. 4(b)). Good single-molecule spectra were obtained with both longitudinal and transverse ultrasonic waves, as will be demonstrated below.

The two traces in Fig. 11(a) show SFS spectra taken at the center of the O_1 band (592.321 nm) using a modulation with transverse ultrasound at a frequency of 4.9 MHz. The sample was bonded to an AT-cut quartz transducer of 1 inch diameter, which carried

highly reflective gold electrodes on both sides. The light reflected off the transducer (which passed through the sample twice) was focussed onto the photodetector. As expected, the resulting SFS spectra were somewhat more reproducible than for the FM/Stark case. Upon proceeding out in the wings of the inhomogeneous line, the SFS amplitude was observed to decrease until multiple-molecule and then single-molecule spectra were observed. The traces (b) through (e) show scans over a spectral region at the blue edge of O_2 (592.004 nm). These spectra were recorded using different light modulation frequencies of 91 MHz (b), 76 MHz (c), 61 MHz (d), and 51 MHz (e). Although the signal-to-noise ratio is somewhat worse than the FM/Stark case (due to the averaging of only 128 scans for each trace), a "W"-like single-molecule signal is clearly visible in all of these traces. As ν_m is decreased, the "W" line shape contracts such that the distance between the downward and the upward slope is always equal to $2\nu_m$. The fiducial bars above the traces mark these distances. The fact that a change of ν_m causes a symmetrical contraction or expansion is the final proof that the "W"-like spectral features that we observe are really due to single molecules (or several molecules absorbing at exactly the same frequency). If these signals were composed of spectral features arising from several molecules at several wavelengths, they would not change in such a systematic manner. The SFS signal at the line center, for instance, does not exhibit well-defined changes when ν_m is varied. The possibility that the "W"-like line shapes are generated by more than one molecule absorbing at exactly the same wavelength, on the other hand, cannot be totally ruled out, but this seems extremely unlikely so far away from the center of the inhomogeneous distribution (compare the estimate of the $\overline{N}_{II}$ values in Section IV.A).

The last two pairs of traces in Fig. 11, (f) and (g), are spectra recorded very far away from the pentacene absorption lines (at 590.452 nm) and scans with no light falling on the detector, respectively. The comparison between (f) and (g) shows that the sensitivity of our double-modulation method is limited by light-related noise (f) which is distinctly larger than the background noise of the electronics (g). However, as was mentioned earlier, our

measurement is not fully quantum-limited but contains a contribution from the avalanche noise of the detector.

At this point a comment on the amplitude of the single-molecule signals as compared to the FM/Stark method may be made. The signal-to-noise ratio in Fig. 11(b) through (e) is smaller than that of our best FM/Stark data (see Fig. 9 (b)) by more than a factor of two that can be explained by the difference in averaging time. The most probable reason is that the ultrasound shifts the center frequencies of the absorption lines by a smaller amount than the electric field. This corresponds to a smaller modulation index m of the secondary modulation and, according to Eq. (10), results in a decrease of the signal amplitude which linearly depends on m. The data shown in Fig. 11 were taken using a power level of -15 dBm to drive the ultrasonic transducer. This level gave the largest SFS signals at the centers of the absorption bands. Higher driving powers resulted only in a broadening and, eventually, in a decrease of the SFS signals. A possible reason for this behavior is the build-up of incoherent ultrasound in the sample due to reflections at the free surface[23] and/or possible heating effects. A proper acoustic termination should help to improve the former problem in future measurements.

In the case of secondary modulation with transverse ultrasound, the signal-to-noise ratio was worse than that for the FM/Stark technique, probably due to a smaller modulation index m (see above). The repeatability of the spectra was improved, however. In order to test if the signal size could be increased by using longitudinal rather than transverse ultrasound, we replaced the AT-cut quartz transducer by a X-cut transducer at 5 MHz. This transducer had no electrodes so that a special sample holder assembly was required for exciting the ultrasonic oscillations. We sandwiched the transducer between two ITO-coated glass plates with the coated sides next to the transducer. In order to achieve a good mechanical contact we placed thin layers of Nonaq stopcock grease between the elements of this stack. The sample was then bonded to the outer side of one of the glass plates with phenyl salicylate.

The advantage of this configuration as compared to the use of a coated transducer was its optical transparency and lower optical losses due to scattering in the sample.

Several typical spectra obtained with longitudinal ultrasonic modulation are displayed in Figure 12. All the traces were obtained by averaging 128 single scans. The structure of the figure is similar to that of Fig. 11. The two traces labeled (a) show strong SFS near the center of the O_1 line (at 592.312 nm). As in the case of transverse ultrasound, the power level of the secondary modulation was adjusted so as to obtain maximal amplitude of the SFS signal; the optimal value turned out to be -20 dBm. The traces (b) through (d) were taken at the blue edge of the O_2 band (at 591.982 nm) with the same ultrasonic power. Each contains a strong single-molecule signal left of the center and several other repeating features which, again, are probably due to other molecules located outside the focal region of the laser. The rf modulating frequency was varied from 76 MHz (b) to 91 MHz (c) and back to 76 MHz (d). The strong "W"-like feature expands and contracts in accordance with these changes (compare the fiducial bars), giving strong evidence for a single molecule. The changes of the smaller signals, on the other hand, do not follow the frequency variation in a similarly obvious way, which suggests that they are caused by several overlapping out-of-focus molecules. This seems reasonable, because there are much larger portions of the probe volume out of the laser focus than in the tiny focal spot.

The signal-to-noise ratio is clearly better than in the case of transverse ultrasonic modulation and is comparable with the Stark effect experiment at equal averaging times (compare Figs. 9, 11 and 12). The better signal-to-noise ratio suggests that the molecular absorption lines are more efficiently shifted by the periodic compression and rarefaction connected with a longitudinal wave than by a shear wave.

The two traces in Fig. 12 (c) were taken way off the O_2 line at 590.741 nm, and these scans do not contain repeatable signals above the noise level. In a manner similar to the Stark and transverse ultrasonic modulation techniques, this result confirms that far enough

away from the inhomogeneous line center, no pentacene molecules are in resonance with the laser frequency. Although the inhomogeneous distribution falls off in the wings much more slowly than the strict Gaussian law would predict (see above), it definitely reaches zero in a certain distance which is smaller than the frequency difference between the O_2 and O_3 bands of roughly 4 nm. The traces (f) at the bottom of Fig. 12 were taken with no light impinging on the detector; these again show that the noise level of our electronics is smaller than the light-related noise of traces (e).

Considering all the experimental data, a comparison between the amplitudes of the SMD signals in the wings of the inhomogeneous line and the SFS spectra taken near the center of the inhomogeneous line may now be made. Using the known cross section and dilution of our samples, we estimated the average number $\overline{N}_H$ of molecular absorption lines per homogeneous linewidth in the probe volume to be on the order of $10^3 - 10^4$ near the band center. If we assume that the number fluctuations $\Delta\overline{N}_H$ roughly scale as $\sqrt{\overline{N}_H}$ (which underestimates $\Delta\overline{N}_H$ for small $\overline{N}_H$), we expect the amplitude of SFS spectra taken near the center of the inhomogeneous band to be larger than a single-molecule signal by a factor of at least 30 - 100. In part of our experimental data, this difference is much smaller - especially with the FM/Stark technique (see Figs. 9 - 12). An explanation may be that the molecules absorbing at the line center which are located in near-equilibrium positions are subject to strong power broadening and a corresponding reduction of their peak absorption cross section. In Sec. III we calculated the saturation light intensity for pentacene in *p*-terphenyl to be 71 mW/cm^2 whereas the actual intensity in our focal spot (in one sideband) was $\simeq$ 0.85 W/cm^2. Those molecules which absorb out in the wings, on the other hand, can be assumed to sit in highly strained sites and may have a higher effective saturation intensity. Evidence for this hypothesis comes also from the absolute magnitude of our SMD signals (see Sec. III).

Another possible reason for the amplitude of our SMD signals could, in principle, be that they are due to pentacene dimers rather than monomers. Even in very dilute solutions of the dye, a certain amount of dimers can be expected to occur, since the solubility in the molten phase during sample preparation is not perfect. There are dimer absorption origins both to the red of the O_1 and to the blue of the O_2 monomer bands[28]. However, the intersystem-crossing rates k_{23}, at least of the long-wavelength dimer states, are much higher than those of the O_1 and O_2 monomers[28], which would give rise to even stronger power broadening due to triplet bottleneck effects[30]. No detailed information about the absorption cross sections σ and phosphorescence decay rates k_{31} of various dimers is currently available so that a qualitative calculation of the saturation light intensity cannot be performed. Nevertheless, due to the high intersystem crossing rates, it seems unlikely that dimers are the origin of our strong SMD signals.

One might argue that it should be possible to test experimentally if a single molecule is subject to strong pumping (i.e., AC Stark effects) by the laser light field or not. If the molecule interacts with a strong light field, its absorption line is expected to split into two components, one positive and one negative, whose separation and relative amplitudes depend on the intensity and frequency detuning of the light from the molecular resonance frequency[36]. This effect, which was first demonstrated in sodium vapor, [37] cannot easily be observed for dye molecules embedded in a solid, since, due to the inhomogeneous distribution, the molecular line doublets are smeared out to one power-broadened line. For one single molecule, however, it should in principle be possible to observe the line splitting. However, our FM scheme is not capable of achieving this for the following reason. In our experiment, the molecular absorption line is saturated by the carrier frequency and probed by the two sidebands. In the simplest case we can assume that the sidebands are weak enough that they do not cause strong pumping. The FM signal is generated (in the S_1 phase) by subtracting the absorption experienced by the upper sideband from that experienced by the lower sideband. Since all three frequencies including the carrier are scanned

simultaneously, the splitting of the absorption line caused by the saturating carrier changes during the scanning process. The resulting FM signal is the same as for a regular power-broadened Lorentzian line, as we have checked by model calculations. The shape of a single-molecule signal in our FM/Stark or FM/US double-modulation experiment does, therefore, not reveal any strong-pumping effects. Future work should consider whether or not strong pumping effects can be detected by operating in the dispersion-sensitive (S_2) phase.

V. Summary and Conclusion

In the present paper we have demonstrated the possibility of detecting the absorption signal of one individual dye molecule in a transparent matrix. Our model system was pentacene in a *p*-terphenyl single crystal at 1.5 K. In order to select one single absorption line we chose rather dilute dopant concentrations between 2×10^{-7} and 1×10^{-6} mole/mole and investigated spectral regions out in the wings of the inhomogeneous O_1 and O_2 absorption bands corresponding to the electronic $|S_1> \leftarrow |S_0>$ (0 - 0) transition. Our detection method was based on laser FM spectroscopy with modulation frequencies between 50 and 100 MHz. Since in this technique weak signals are often obscured by residual amplitude modulation (RAM), we used a secondary modulation of the absorption lines of the sample by applying either an electric ac field or transverse or longitudinal ultrasonic waves. With each of these three double-modulation methods we achieved a detection sensitivity close to the quantum noise limit and unambiguously observed single-molecule signals. This rules out the possibility of artifacts that might arise if only one technique is used. In order to obtain a favorable signal-to-noise ratio, we chose to tolerate some power broadening of the absorption lines. However, the absolute amplitude of the SMD signals as well as its relation to the magnitude of SFS recorded near the centers of the inhomogeneous bands led to the conclusion that molecules absorbing out in the wings have

a higher saturation light intensity than those at the center. This may indicate that the presence of high local strains at the single-molecule sites alters the intersystem crossing rates.

The spectroscopic detection and study of single dye molecules in a solid may lead to a variety of novel experimental studies in the future. One direction could be the measurement of the photophysical properties of the dopant molecules themselves, such as lifetimes and transition rates. In this context, it would be interesting to repeat the experiments reported here on samples with much lower pentacene concentrations, in which single-molecule spectra could be detected closer to the centers of the inhomogeneous origins. By investigating power broadening behavior, it should be possible to obtain information about the influence of the matrix environment on intramolecular relaxation channels, especially on the intersystem crossing rate.

Another application of single-molecule spectroscopy could be the extremely site-selective investigation of small changes in the matrix, in which case the dopant *molecule acts only* as a probe. An example is persistent spectral hole-burning on one molecule, which might help to elucidate the hole-burning mechanism in the pentacene / *p*-terphenyl system. Since pentacene is a fairly photostable molecule for long-wavelength irradiation at low temperatures, the mechanism probably involves a structural or orientational rearrangement of a nearby matrix molecule. Other studies of the influence of the local environment could be accomplished by measuring the effects of external perturbations (excluding of course the external field required to detect the absorption).

If SMD can be realized in amorphous dye-matrix systems, an interesting application might be the microscopic study of spectral diffusion [38,39]. This phenomenon is a spectroscopic manifestation of slow relaxation processes that are common in non-equilibrium solids such as glasses. In hole-burning experiments, spectral diffusion leads to broadening of a hole with a logarithmic time dependence[40]. One single molecular absorption line, on the other hand, is expected to perform a random-walk-like motion. It would be necessary,

however, to find an amorphous dye-matrix system with an extremely low hole-burning quantum yield, so that the center can be observed over a sufficiently long period of time.

In general, the optical detection of single molecules in a solid removes any effects of inhomogeneous broadening which, to some extent, are still present in conventional site-selective methods of spectroscopy such as persistent spectral hole-burning and coherent transients. It is therefore capable of investigating dye-matrix interactions in a truly local manner, since the usual averaging over many dopant molecules with accidentally degenerate transition frequencies is absent.

ACKNOWLEDGEMENT

The authors thank G. C. Bjorklund and J. G. Miller for valuable discussions, A. Dewey for the loan of the optical storage objective lens, K. Kanazawa for the loan of several quartz transducers, and H. Looser and V. Lee for assistance with sample preparation. This work was supported in part by the U. S. Office of Naval Research and the IBM World Trade Organization.

REFERENCES

1. A. M. Portis, Phys. Rev. 91, 1071 (1953).
2. A. M. Stoneham, Rev. Mod. Phys. 41, 82 (1969).
3. W. E. Moerner and T. P. Carter, Phys. Rev. Lett. 59 , 2705 (1987); W. E. Moerner and T. P. Carter, Bull. Am. Phys. Soc. 32, 1630 (1987).
4. T. P. Carter, M. Manavi, and W. E. Moerner, J. Chem. Phys. 89, 1768 (1988).
5. T. P. Carter, D. E. Horne, and W. E. Moerner, Chem. Phys. Lett. 151, 102 (1988).
6. W. M. Itano, J. C. Bergquist, and D. J. Wineland, Science 237, 612 (1987) and refs. therein.
7. J. C. Bergquist, R. G. Hulet, W. M. Itano, and D. J. Wineland, Phys. Rev. Lett. 57, 1699 (1986).
8. F. Diedrich and H. Walther, Phys. Rev. Lett. 58, 203 (1987).
9. F. Diedrich, J. Krause, G. Rempe, M. O. Scully, and H. Walther, IEEE J. Quant. Elect. 24, 1314 (1988).
10. W. M. Itano, J. C. Bergquist, R. G. Hulet, and D. J. Wineland, Phys. Rev. Lett. 59, 2732 (1987).
11. J. C. Bergquist, W. M. Itano, and D. J. Wineland, Phys. Rev. A 36, 428 (1987).
12. D. J. Wineland, W. M. Itano, and J. C. Bergquist, Optics Lett. 12, 389 (1987).
13. A. Ashkin and J. M. Dziedzic, Science 235, 1517 (1987).
14. D. C. Nguyen, R. A. Keller, J. H. Jett, and J. C. Martin, Anal. Chem. 59, 2158 (1987).
15. R. Lange, W. Grill, and W. Martienssen, Europhys. Lett. 6, 499 (1988).
16. W. E. Moerner and L. Kador, Phys. Rev. Lett. 62, 2535 (1989).
17. G. C. Bjorklund, Opt. Lett. 5, 15 (1980).
18. E. A. Whittaker, M. Gehrtz, and G. C. Bjorklund, J. Opt. Soc. Am. B 2, 1320 (1985).

19. M. Romagnoli, M. D. Levenson, and G. C. Bjorklund, J. Opt. Soc. Am. B 1, 571 (1984).

20. M. Gehrtz, G. C. Bjorklund, and E. A. Whittaker, J. Opt. Soc. Am. B 2, 1510 (1985).

21. E. A. Whittaker, B. J. Sullivan, G. C. Bjorklund, H. R. Wendt, and H. E. Hunziker, J. Chem. Phys. 80, 961 (1984).

22. A. L. Huston and W. E. Moerner, J. Opt. Soc. Am. B 1, 349 (1984).

23. W. E. Moerner and A. L. Huston, Appl. Phys. Lett. 48, 1181 (1986).

24. G. C. Bjorklund, M. D. Levenson, W. Lenth, and C. Ortiz, Appl. Phys. B 32, 145 (1983).

25. J. H. Meyling and D. A. Wiersma, Chem. Phys. Lett. 20, 383 (1973).

26. R. W. Olson and M. D. Fayer, J. Phys. Chem. 84, 2001 (1980).

27. H. de Vries and D. A. Wiersma, J. Chem. Phys. 70, 5807 (1979).

28. F. G. Patterson, H. W. H. Lee, W. L. Wilson, and M. D. Fayer, Chem. Phys. 84, 51 (1984).

29. R. C. Hilborn, Am. J. Phys. 50, 982 (1982).

30. H. de Vries and D. A. Wiersma, J. Chem. Phys. 72, 1851 (1980).

31. H. de Vries and D. A. Wiersma, J. Chem. Phys. 69, 897 (1978).

32. R. H. Pantell and H. E. Puthoff, *Fundamentals of Quantum Electronics* (Wiley, New York, 1969), p. 73.

33. J. H. Meyling, W. H. Hesselink, and D. A. Wiersma, Chem. Phys. 17, 353 (1976).

34. F. P. Chen, S. J. Sheng, and D. M. Hanson, Chem. Phys. 5, 60 (1974).

35. L. Kador and D. Haarer, J. Appl. Phys. 62, 4226 (1987).

36. Y. R. Shen, Principles of Nonlinear Optics (Wiley, New York, 1984), pp. 413-436.

37. F. Y. Wu, S. Ezekiel, M. Ducloy, and B. R. Mollow, Phys. Rev. Lett. 38, 1077 (1977).

38. J. L. Black and B. I. Halperin, Phys. Rev. B 16, 2879 (1977).

39. T. L. Reinecke, Sol. St. Comm. 32, 1103 (1979).

40. W. Breinl, J. Friedrich, and D. Haarer, J. Chem. Phys. 81, 3915 (1984).

FIGURE CAPTIONS

Figure 1. Structure of an inhomogeneously broadened absorption line (upper part) and principle of single-molecule detection (lower part) in a schematic representation. The inhomogeneous line is the envelope of many accumulated molecular zero-phonon (homogeneous) absorption lines arising from absorbing molecules in a transparent matrix. Near the center, the inhomogeneous band is approximately Gaussian, whereas far out in the wings single homogeneous lines are present. The lower part shows cross sections through the sample with the waist of a focussed laser beam. At the line center, many dye molecules are located in the path of the beam, out in the wings very few molecules (ideally: one single) are probed.

Figure 2. Schematic of a simple FM experiment. The top of the figure shows the light spectrum at the output of the laser, after the electro-optic modulator crystal, and after the sample (from left to right), the arrows indicating the relative phases of the electric light fields. For a discussion see text. More detailed diagrams of our double-modulation techniques are depicted in Figs. 3, 4(a), and 4(b).

Figure 3. Optical setup used in the SMD experiments. For the connections of the first-stage local oscillator LO1, the external drive for the sample modulation, and the output signals of the photodiodes PD1 and PD1R, see Figs. 4(a) and 4(b). The symbols are explained in the text.

Figure 4(a). Schematic showing the processing of the signals of the photo-diodes PD1 and PD1R in the FM/Stark experiment (compare Fig. 4(b)). The first-stage demodulation (with respect to the laser FM) is performed by the mixers M1, the second-stage demodulation (with respect to the electric-field modulation of the sample) by the lock-in amplifier LiA. Two

different high-voltage sources HV were used which provided either a sinusoidal waveform or a bipolar square wave. For the explanation of the other symbols see the text.

Figure 4(b). Schematic showing the processing of the signals of the photo-diodes PD1 and PD1R in the FM/US experiment (compare Fig. 4(a)). The first-stage demodulation (with respect to the laser FM) is performed by the mixers M1, the second-stage demodulation (with respect to the ultrasonic modulation of the sample) by mixer M2. For the explanation of the other symbols see text.

Figure 5. Theoretical double-modulation line shapes. (a) A broad Lorentzian absorption; (b) FM - S_1 signal for (a); (c) Double modulation - S_1 signal for (a); (d) Double modulation - S_1 signal for a narrower Lorentzian, (e) Dispersion signal for (a); (f) FM - S_2 signal for (a); (g) Double modulation - S_2 signal for (a); (h) Double modulation - S_2 signal for a narrower Lorentzian. All y-axis scales have been normalized for clarity, with zero signal at the center of each y axis.

Figure 6. Persistent spectral holes for pentacene in *p*-terphenyl detected using simple FM with $\omega_m/2\pi = 75$ MHz. (a) Hole just after burning, (b) Applied dc field of 28 kV/cm, (c) Applied dc field of 45 kV/cm, (d) Back to zero field.

Figure 7. Spectral holes detected using simple FM and FM/Stark double modulation. (a) Hole in simple FM, $\nu_m = \omega_m/2\pi = 75$ MHz , S_1 phase. (b) FM/Stark, S_1 phase, $\nu_m = 75$ MHz, 2f detection. (c) $\nu_m = 90$ MHz. (d) S_2 phase, $\nu_m = 75$ MHz. (e) $\nu_m = 90$ MHz.

Figure 8. Variations in SFS and αL over the O_1 and O_2 bands. The circles represent mean-square values of SFS over 0.5 GHz spectral ranges. The solid line is the measured

absorptance from a higher-concentration sample. The arrows mark the approximate spectral ranges in which single-molecule spectra were recorded.

Figure 9. Single-molecule spectra using FM/Stark technique (quadratic Stark effect) (a) Simulation of FM/Stark lineshape. (b) SMD spectra at 592.455 nm, 512 averages, 8 traces overlaid, bar shows value of $2\nu_m$ = 150 MHz. (c) Average of traces in (b) (S_2 removed) with fit to the in-focus molecule (smooth curve). (d) Signal far off line at 597.514 nm. (e) Signal at O_1 line center (592.326 nm) for an undoped *p*-terphenyl crystal. (f) Traces of SFS at the O_2 line center (592.186 nm) for the doped crystal.

Figure 10. FM/Stark spectra with second-stage demodulation sensitive to a linear Stark effect. (a) Eight overlaid spectra at 592.057 nm, ν_m = 50 MHz, 512 scans averaged for each. (b) Average of the eight traces in (a). (c) Spectra way off line at 593.071 nm. (d) Strong SFS at O_2 line center, 592.192 nm.

Figure 11. FM/US spectra with transverse (shear) ultrasound, 128 averages each. (a) SFS at O_1 line center (592.321 nm) (b) SMD, S_1 phase, ν_m = 91 MHz, 592.004 nm. (c) Same region, ν_m = 76 MHz (d) Same region, ν_m = 61 MHz (e) Same region, ν_m = 51 MHz (f) Far away from the pentacene absorption lines, 590.452 nm. (g) No light on the detector.

Figure 12. FM/US spectra with longitudinal ultrasound for secondary modulation, 128 averages each. (a) SFS near O_1 line center with ν_m = 76 MHz, 592.312 nm. (b) SMD at 591.982 nm, ν_m = 76 MHz (c) ν_m = 91 MHz (d) ν_m = 76 MHz (e) Way off line, 590.741 nm. (f) No light on the detector.

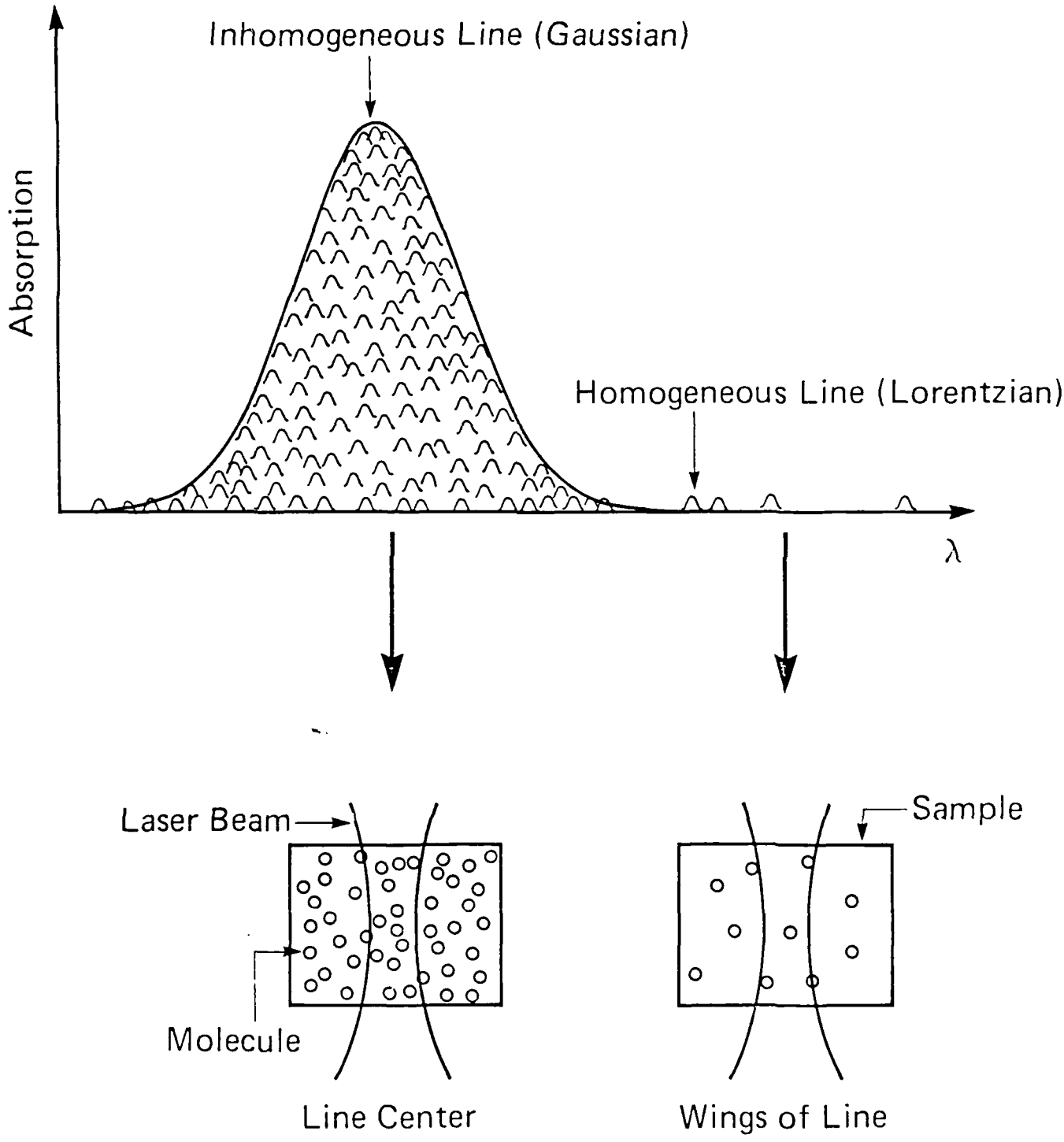
Inhomogeneous Line (Gaussian)
Absorption
Homogeneous Line (Lorentzian)
λ
Laser Beam
Sample
Molecule
Line Center
Wings of Line

Figure 1

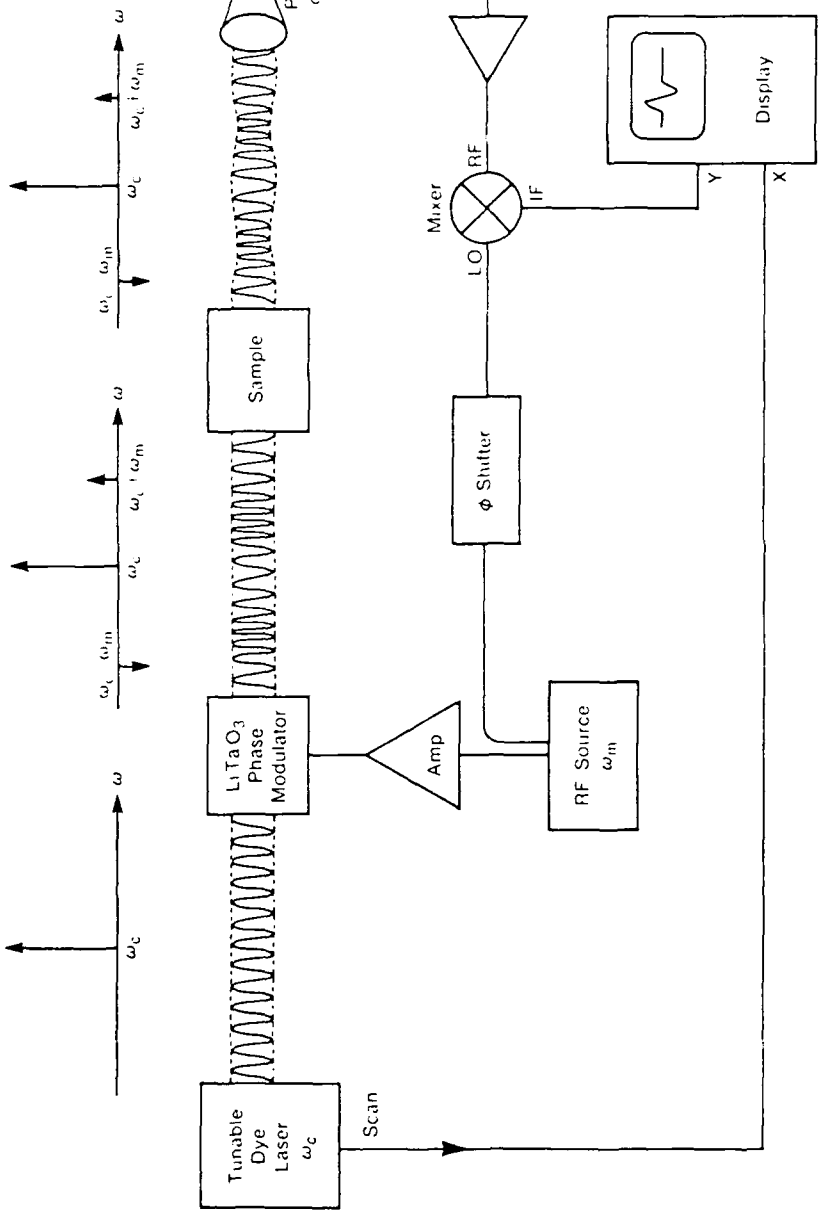
Tunable Dye Laser ω_c
Scan
$LiTaO_3$ Phase Modulator
Amp
RF Source ω_m
Sample
Photo-diode
Mixer
RF
IF
LO
ϕ Shifter
Display
Y
X
ω_c
$\omega_c \pm \omega_m$

Figure 2

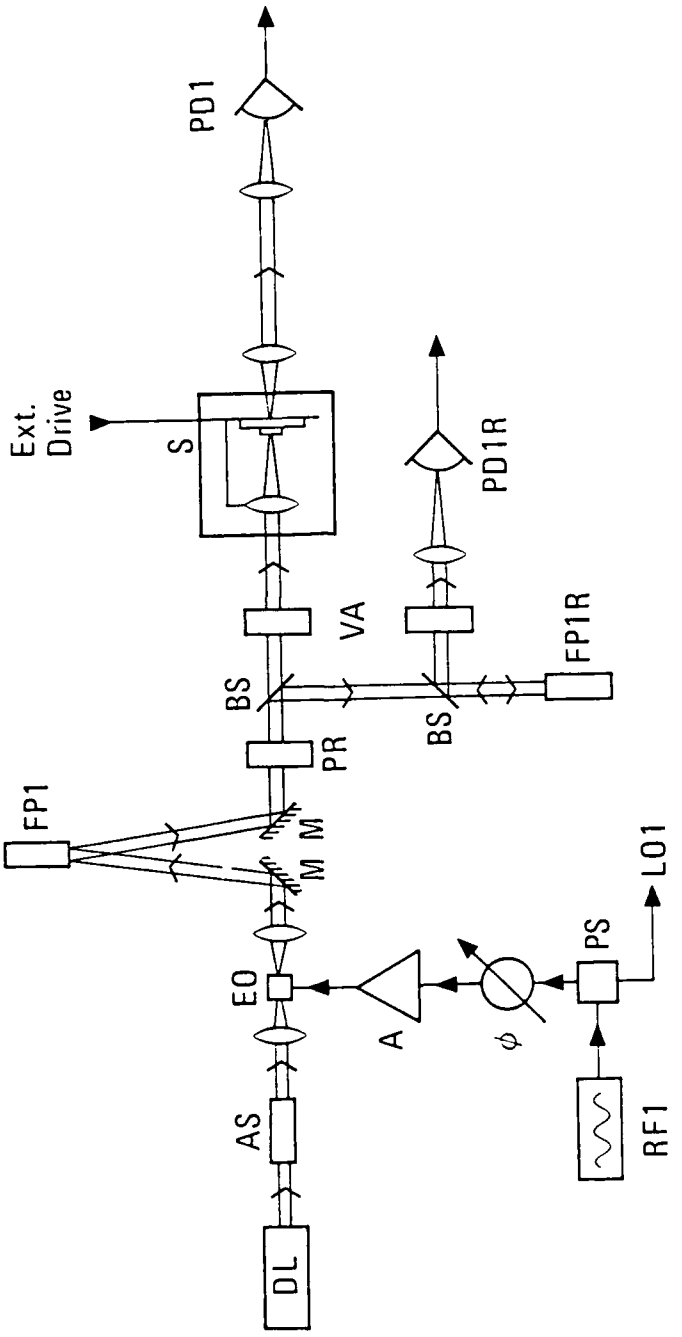

Figure 3

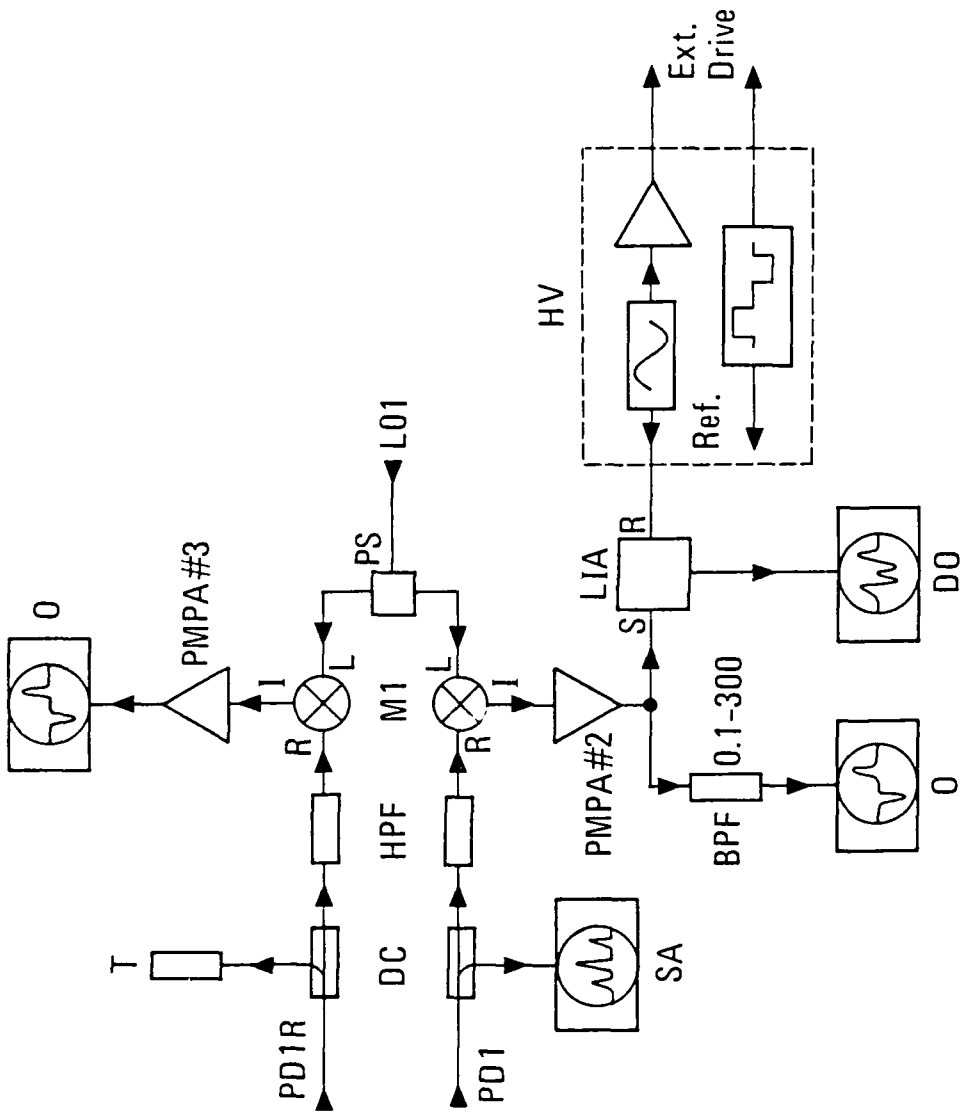
Ext.
Drive
HV
Ref.
LIA
R
S
DO
0
BPF
0.1-300
PMPA#2
PS
LO1
PMPA#3
0
I
L
R
M1
L
R
I
HPF
DC
T
PD1R
PD1
SA

Figure 4 (a)

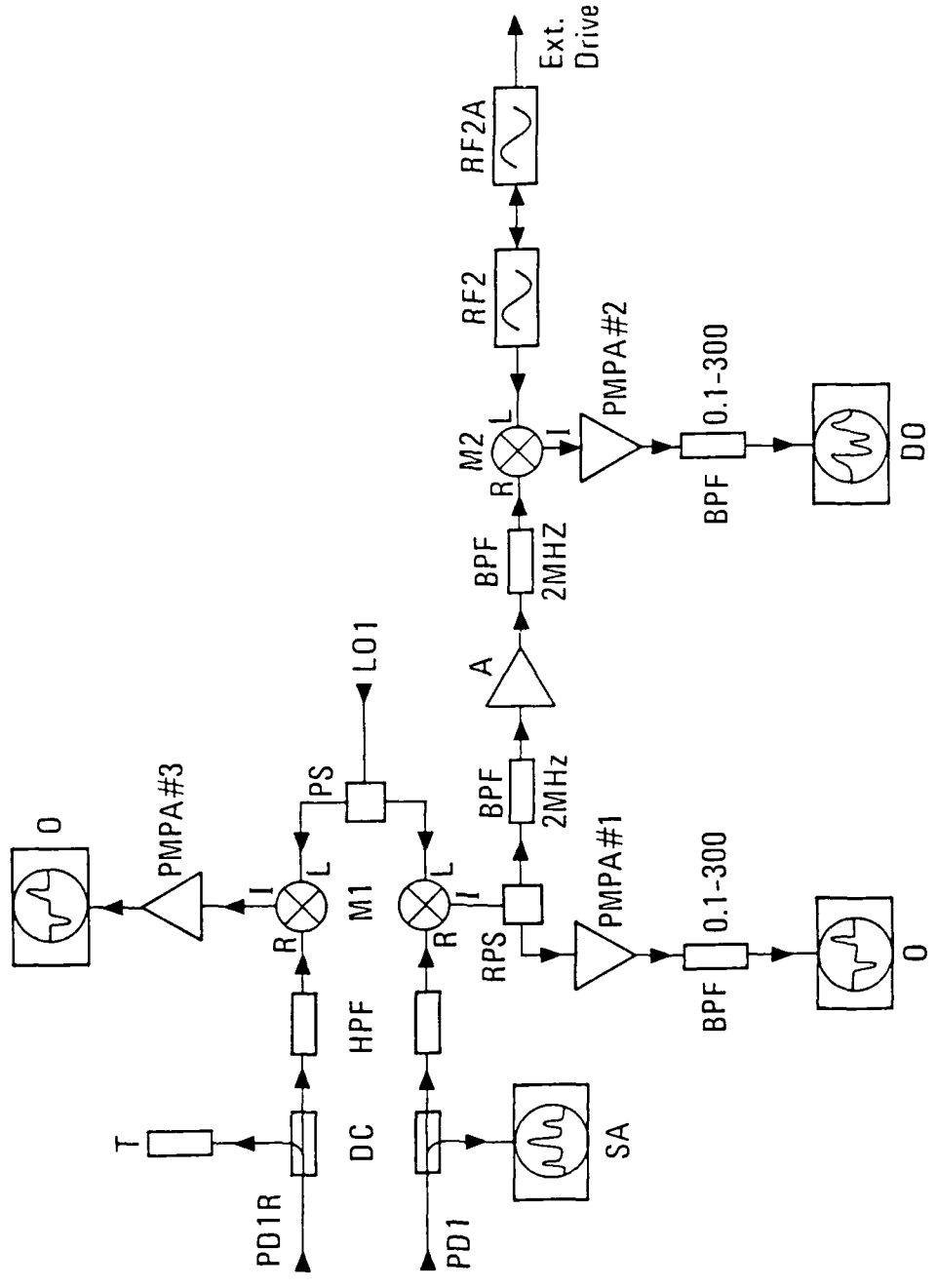
Ext.
Drive
RF2A
RF2
M2
PMPA#2
BPF
0.1-300
DO
BPF
2MHZ
A
LO1
PS
BPF
2MHz
PMPA#3
O
M1
PMPA#1
BPF
0.1-300
O
RPS
T
DC
HPF
SA
PD1R
PD1

Fibure 4 (b)

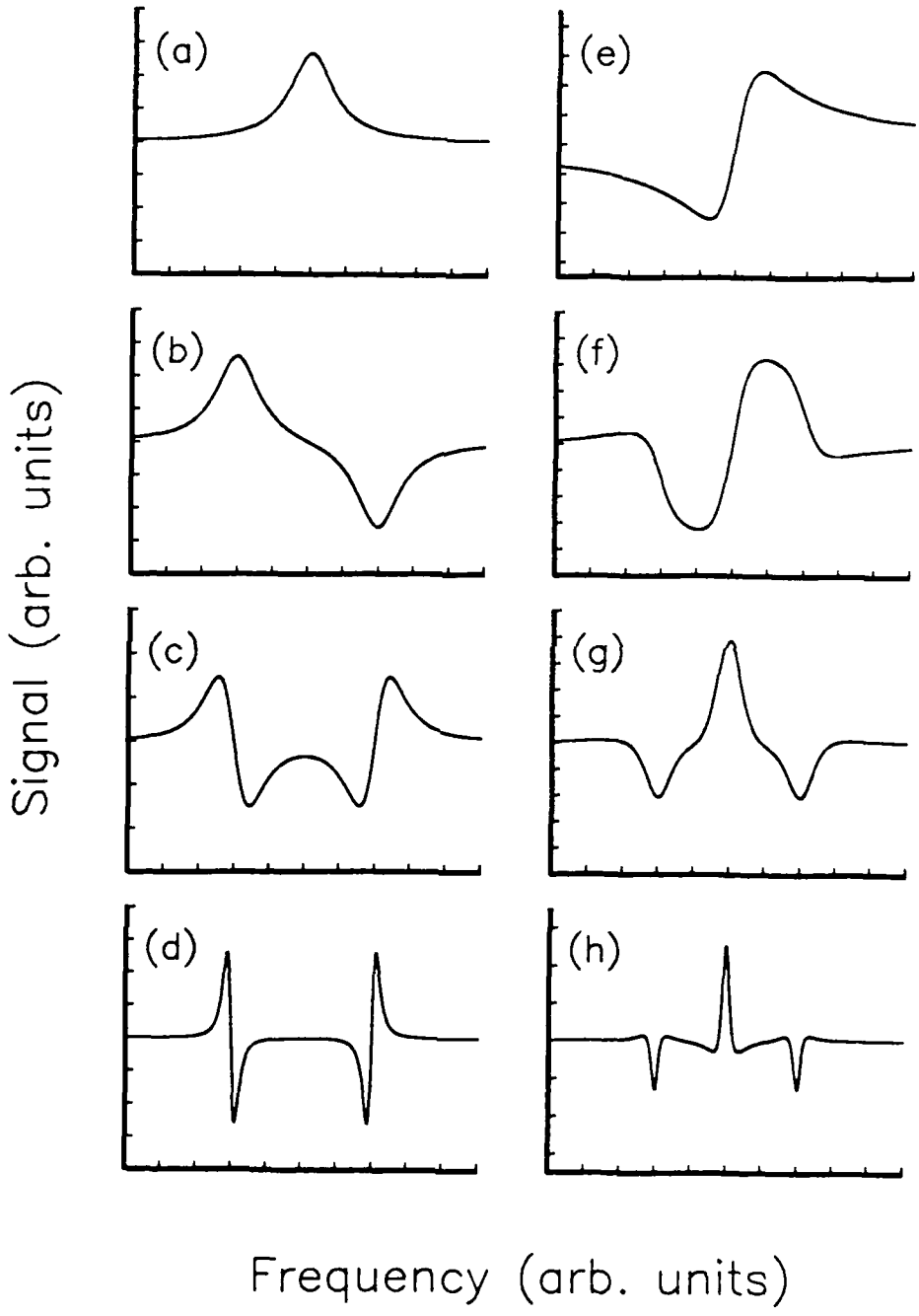

Figure 5

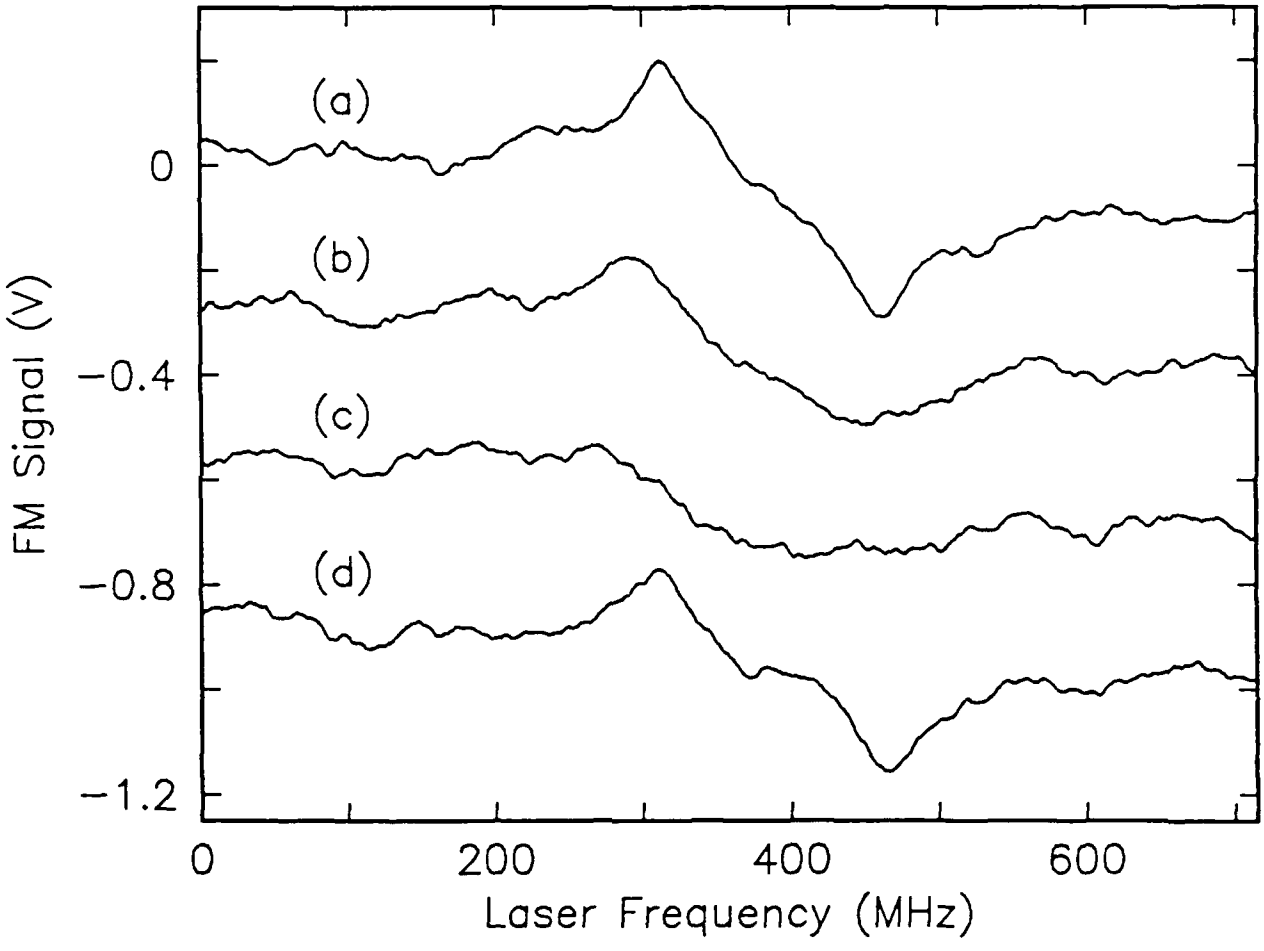

Figure 6

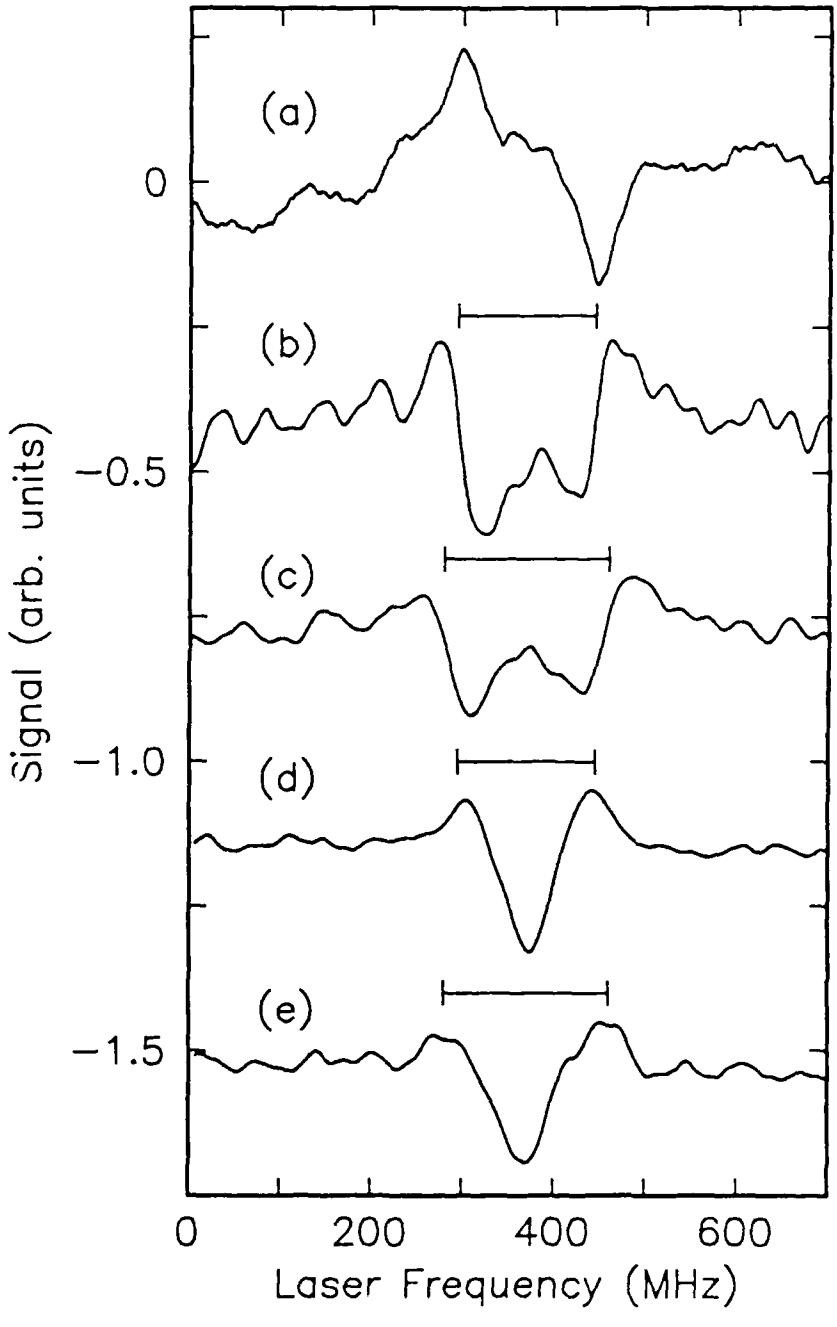
(a)
(b)
(c)
(d)
(e)
0
−0.5
−1.0
−1.5
Signal (arb. units)
0
200
400
600
Laser Frequency (MHz)

Figure 7

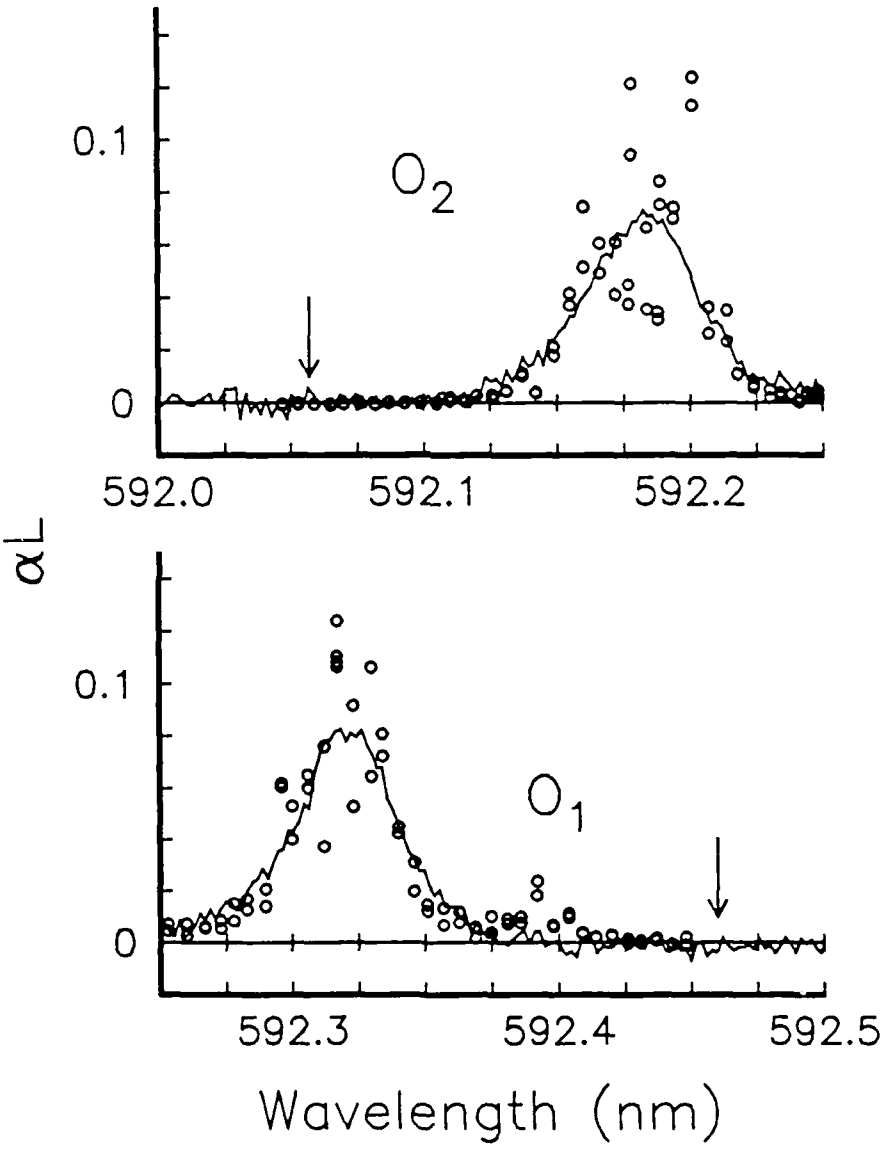

Figure 8

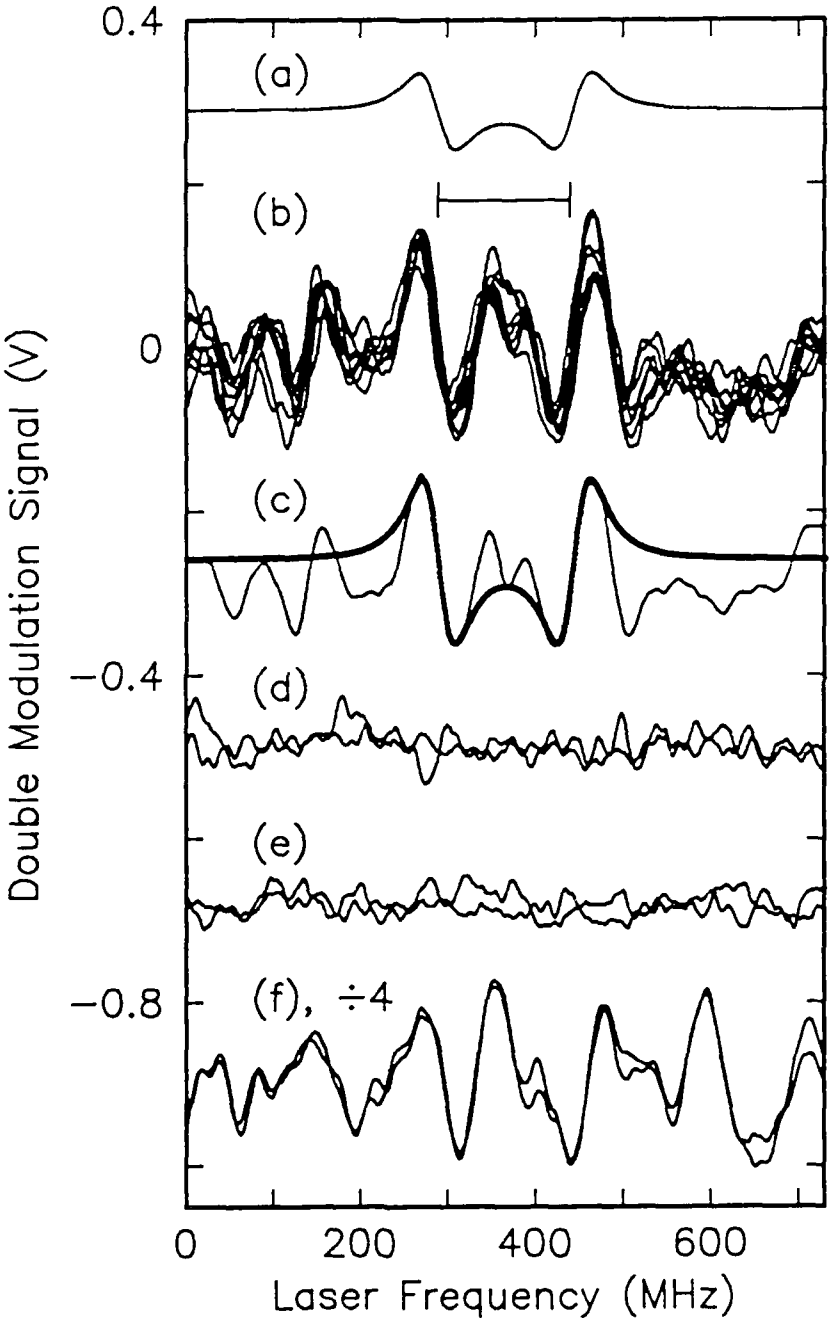
0.4
(a)
(b)
0
(c)
−0.4
(d)
(e)
−0.8
(f), ÷4
Double Modulation Signal (V)
0
200
400
600
Laser Frequency (MHz)

Figure 9

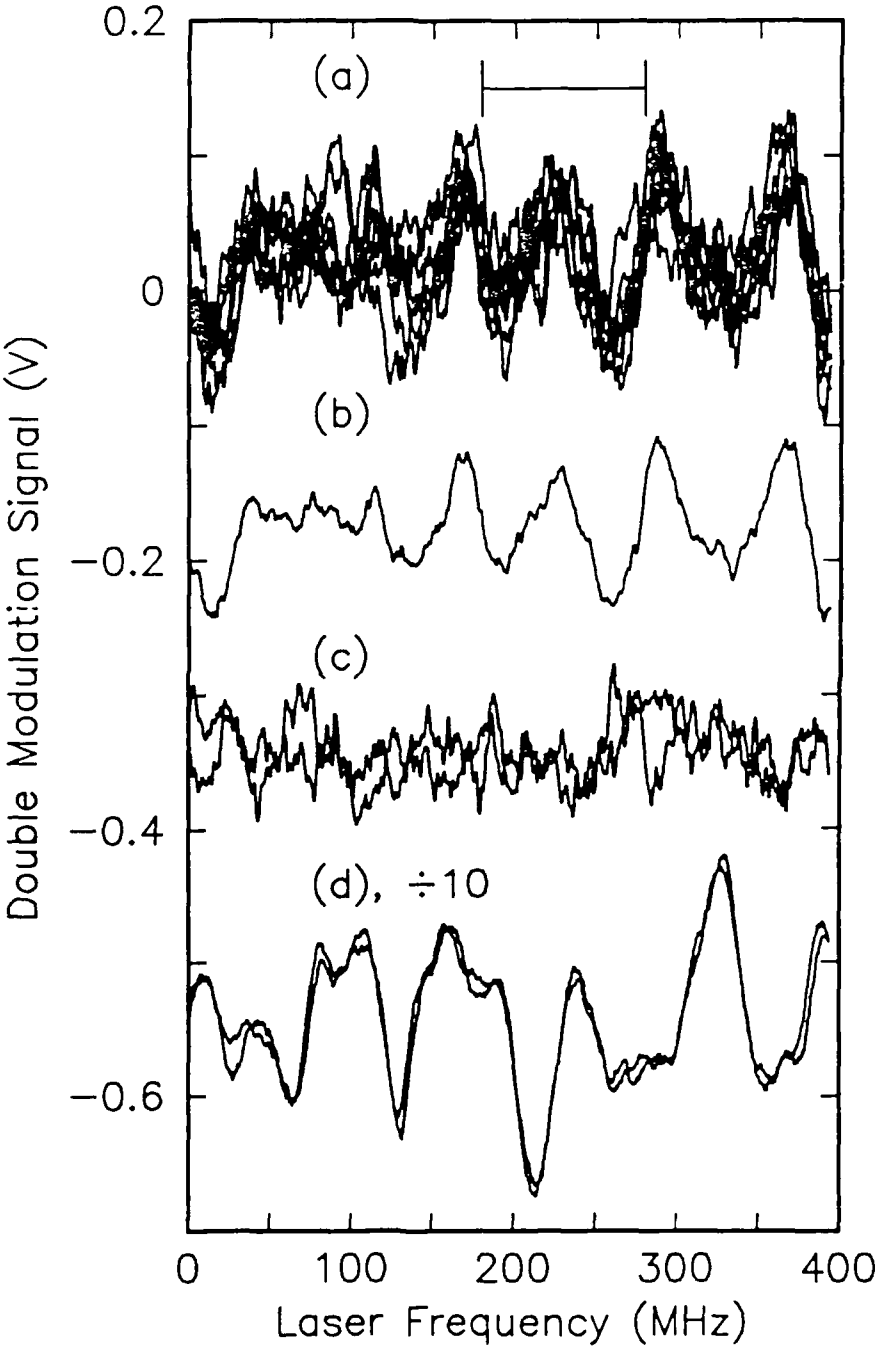
0.2
0
−0.2
−0.4
−0.6
(a)
(b)
(c)
(d), ÷10
Double Modulation Signal (V)
0
100
200
300
400
Laser Frequency (MHz)

Figure 10

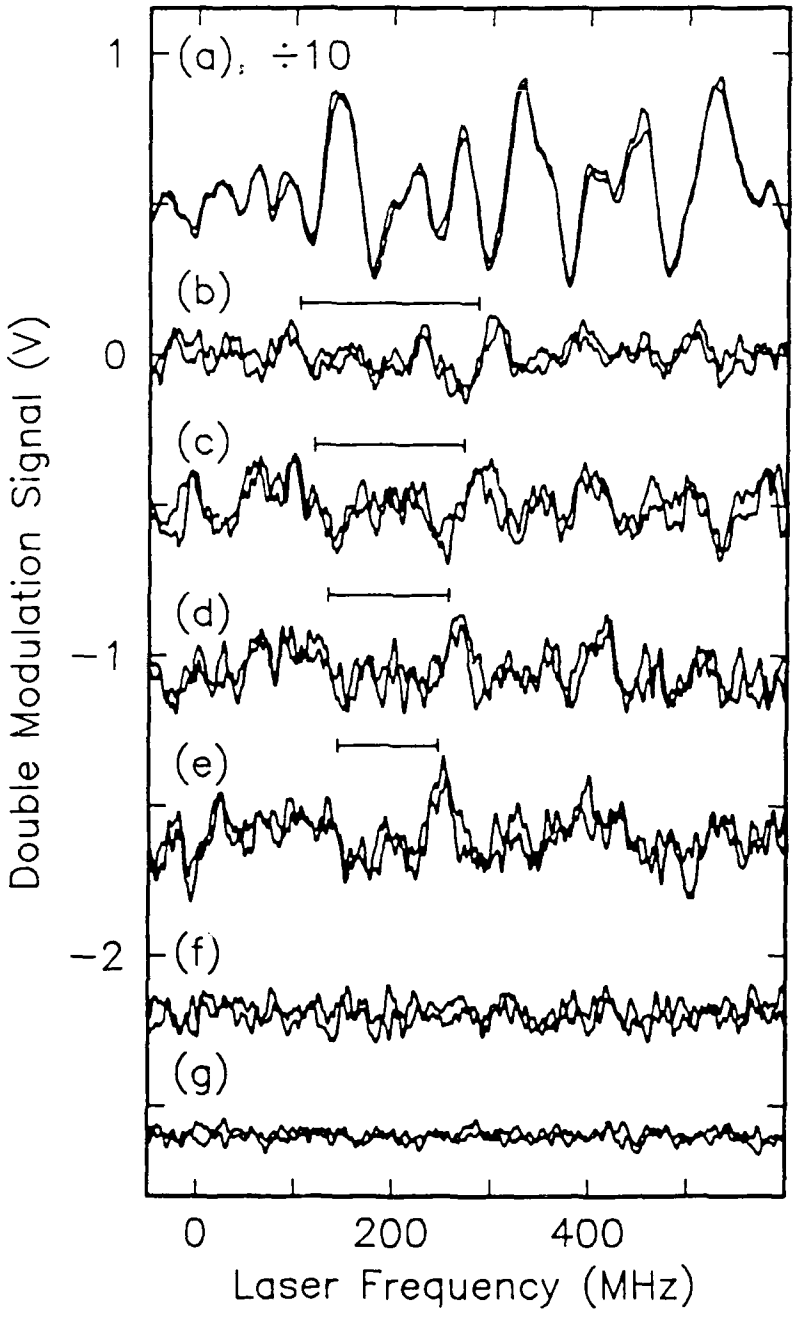
(a), ÷10
(b)
(c)
(d)
(e)
(f)
(g)
1
0
−1
−2
Double Modulation Signal (V)
0
200
400
Laser Frequency (MHz)

Figure 11

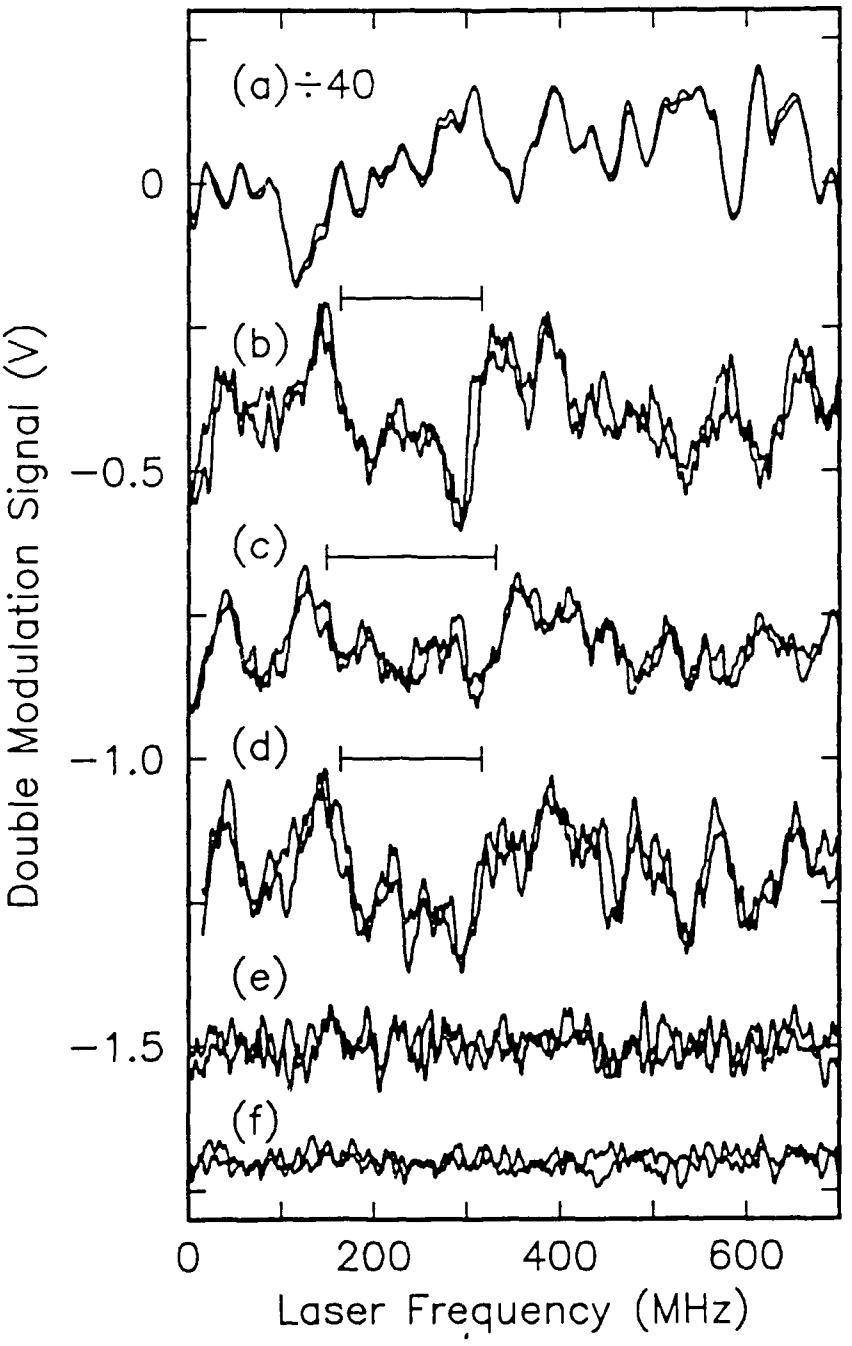
(a)÷40
(b)
(c)
(d)
(e)
(f)
0
−0.5
−1.0
−1.5
Double Modulation Signal (V)
0
200
400
600
Laser Frequency (MHz)

Figure 12

DL/1113/89/1

TECHNICAL REPORT DISTRIBUTION LIST, GENERAL

	No. Copies
Office of Naval Research Chemistry Division, Code 1113 800 North Quincy Street Arlington, VA 22217-5000	3
Commanding Officer Naval Weapons Support Center Attn: Dr. Bernard E. Douda Crane, IN 47522-5050	1
Dr. Richard W. Drisko Naval Civil Engineering Laboratory Code L52 Port Hueneme, California 93043	1
Defense Technical Information Center Building 5, Cameron Station Alexandria, Virginia 22314	2 high quality
David Taylor Research Center Dr. Eugene C. Fischer Annapolis, MD 21402-5067	1
Dr. James S. Murday Chemistry Division, Code 6100 Naval Research Laboratory Washington, D.C. 20375-5000	1
Dr. Ronald L. Atkins Chemistry Division (Code 385) Naval Weapons Center China Lake, CA 93555-6001	1
Chief of Naval Research Special Assistant for Marine Corps Matters Code 00MC 800 North Quincy Street Arlington, VA 22217-5000	1
Dr. Bernadette Eichinger Naval Ship Systems Engineering Station Code 053 Philadelphia Naval Base Philadelphia, PA 19112	1
Dr. Sachio Yamamoto Naval Ocean Systems Center Code 52 San Diego, CA 92152-5000	1
David Taylor Research Center Dr. Harold H. Singerman Annapolis, MD 21402-5067 ATTN: Code 283	1